FABRICATION AND CHARACTERIZATION OF CO-CONTINUOUS ELASTOMER-HYDROGEL COMPOSITES

BY

QIAN ZHANG

THESIS

Submitted in partial fulfillment of the requirements
for the degree of Master of Science in Mechanical Engineering
in the Graduate College of the
University of Illinois at Urbana-Champaign, 2016

Urbana, Illinois

Adviser:

Assistant Professor Shelby Hutchens

Abstract

The increasing demand of applications in polymer industry requires new or improved combinations of material properties, which cannot be satisfied by few polymers alone. There has therefore been scientific and industrial interest in mixing two different polymers together to make polymer blends [1]. Of all possible polymer blend morphologies, co-continuous blends are of particular interest due to their unique property of possessing two continuous phases [2]. In this research, a co-continuous structured elastomer-hydrogel composite is fabricated to combine the elasticity of elastomer and the permeability of hydrogel. The stretchable, water permeable composite can be used as a mechanically tunable molecular sieve in drug delivery and tissue engineering. Porous PEO-PDMS elastomer with interconnected microchannels is filled with polyacrylamide hydrogels via a microsphere-templating process. The configuration of the microstructure of the composite is observed and analyzed. Besides, the mechanical properties and diffusivity properties of the composite are experimentally characterized. In general, this research provides experimental bases for designing a new polymer blends of elastomer and hydrogel. It also aids in the creation of guidelines for the analysis of elastomer-hydrogel interactions.

Acknowledgment

I would not have been able to complete this research project without the help of many individuals. First, I would like to express my gratitude to my advisor, Professor Shelby Hutchens, for giving me the opportunity and constant advice. I am very grateful for the technical and professional growth I have received under her guidance throughout my Master's research. Next, I would like to thank all my groupmates, Bingyang Zhang, Matthew Paul Milner, Steven Yang, for their friendly discussions and help to my research. They offered assistance in many aspects of this research and provided technical support when the experiments didn't pan out. I would also like to acknowledge the Department of Mechanical Science and Engineering at University of Illinois at Urbana-Champaign.

In addition, I would like to thank my family and friends, thanks for their support and all the memories. I can accomplish nearly anything without support of my parents. Special thanks to my parents for your love, sacrifice, and encouragement.

Table of Contents

List of Figures

List of Tables

Chapter 1

Introduction and Theory of Co-continuous Structured Polymer Blends

1.1 Fundamentals of Polymer Blends

Polymers have been rapidly evolving since the 1930s, and the field of polymer blends has been one of the most prominent areas of investigation in recent research advances. Similar to the development of metal alloys, polymer blends are fabricated by physical mixing of two or more polymers that have different chemical or physical properties. Blending results in desirable different properties inherent to each parent polymer, along with the ability to optimize the behavior of the resulting polymeric composite [3-6]. Thus, the synergistic interactions and tunable material composition allows for improvements in material properties that satisfy broader performance spectra, such as chemical resistance, gas permeability and diffusivity, processability, flame resistance, with rapid product development and deployment [7]. Besides, polymer blends offer the advantages of reducing research and development cost and time, yielding enhanced material properties that may not be easily achieved by a new polymeric structure [3].

The primary differentiation of polymer blends is their phase miscibility, i.e. whether the polymeric phases separate or form a single phase at the molecular scale when mixed together. However, the immiscibility dominates most polymers that show mechanical incompatibility due to the weak adhesion at the phases interfaces. Because even a small difference in physical or chemical characteristics in a polymer chain could make two

components immiscible with each other [8-10]. The performance of incompatibility depends on the ingredients, concentration, and morphology etc. Since polymer blends require stability during the polymer forming process, compatibilization between multicomponent phases plays an important role in the formation of polymer blends.

In general, there are three key methods to achieve the compatibilization. First, the phase morphology can be stabilized against shear or thermal effects during formation process. Conventionally, the polymers are heated above their melting temperatures to form molten liquid state then mixed and quenched to form solidified polymer blends [4]. Because normally polymer has a higher viscosity than air or water so a very slow phase separation process can be accomplished in the solidification process by using an appropriate cooling rate [11]. Second, the compatibilization can be achieved by the improvement of interfacial adhesion between the solid-state phases, such as adding a compatibilizing agent to increase the mutual interaction between polymer phases. More specifically, the addition of compatibilizing agent includes: 1) addition of copolymer in which one segment is miscible with one phase and another with the other phase 2) addition of nanoparticles that can influence polymeric structure 3) addition of compatibilizer that is miscible with both phases 4) addition of reactive compounding that can modify at least one macromolecular species and result in local miscibility regions [11]. Recent novel methods for polymer compatibilization involve mechanochemistry and solid-state mechanics [5]. On the other hand, the addition of a compatibilizing agent into a blend is often constrained by high cost of compatibilizers, poor dispersion, and negative impact on blend performance [12]. The third method is to dissolve the polymers in a solvent to increase the entropy

followed by the rapid removal of the solvent to prevent phase separation hence a single phase can be formed [4].

Polymer blends have sparked in many aspects of contemporary technology, including automotive applications, electronics to applications for energy generation and harvesting, biofuel processing, membrane sciences, and healthcare industry etc. [3, 11]. For example, in healthcare industry hydroxyapatite blended with PLA and PMMA can form a tissue scaffold and used in prosthetics. PP blended with SBR or SEBS can also be used to support necessary body weight and movement for the latter application [13]. Recently, co-continuous structure polymer blends have drawn attentions to tissue engineering because of its unique interconnected structure than other morphological structure of polymer blends. In tissue engineering, a scaffold with a co-continuous structure can be formed by blending two biodegradable polymers together. The co-continuous structure could provide continuous paths for an active drug to be released into the body.

Based on the chemical reaction, material properties, processing conditions etc., there are four main types of phase morphology of polymer blends: droplet-matrix, matrix fiber, lamellar, and co-continuous structure, as shown in Figure 1 [10, 14]. The type of morphology depends on interfacial tension, viscosities ratio, volume fractions, and the processing conditions. Each of phase morphology has been extensively used and studied in various fields, such as self-reinforcing property in droplet-matrix structure and barrier enhancing property in lamellar structure [15, 16]. This research focuses on the co-continuous morphologies because both components in the co-continuous structure can fully contribute to the properties of the blend in all directions.

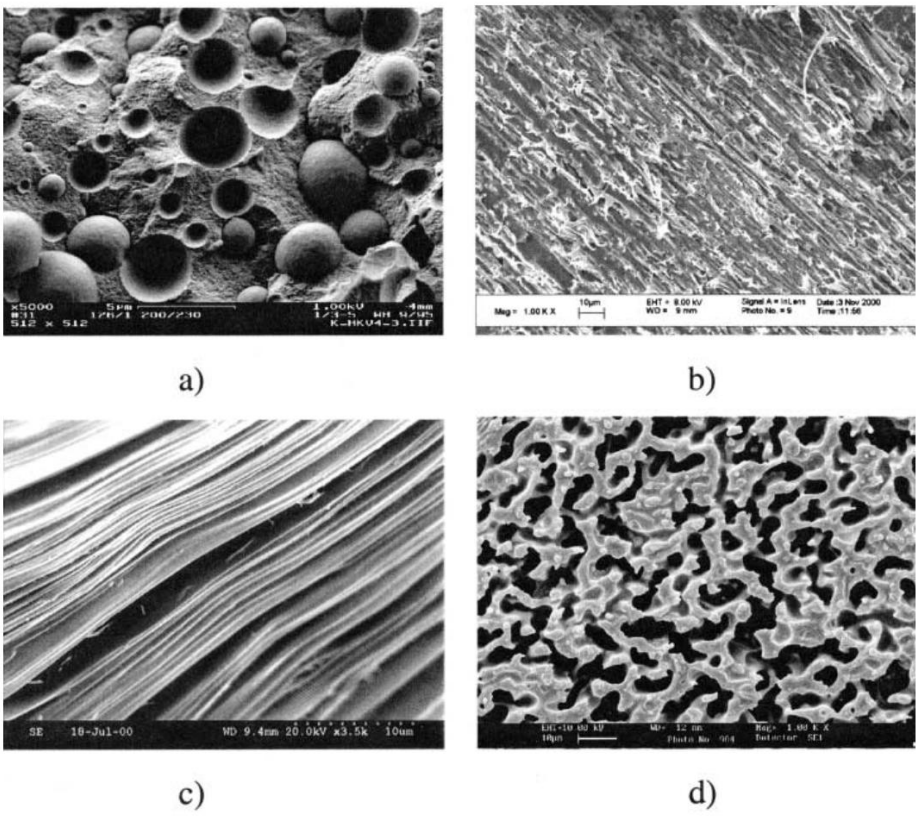

Figure 1: Phase morphology of polymer blends: (a) droplet-matrix structure (b) matrix-fiber structure (c) lamellar structure (d) co-continuous structure [10, 14]

1.2 Co-continuous Structure Polymer Blends

Polymer blends can adopt four types of morphologies: droplet-matrix structure, matrix-fiber structure, lamellar structure, and co-continuous structure. The property of droplet-matrix structure largely depends on the matrix phase. The orientation of the dispersed fibers mainly determines the property of matrix-fiber structure. For the lamellar structure, alternating layers of different materials result in orientation dependent barriers properties. Of the four structures, co-continuous structure is of particular interest because it possesses a unique continuous interpenetrated network. Both components will equally

contribute to the material properties and the isotropic material behavior can be expected. Figure 2 shows an example of a three-dimensional reconstruction of a co-continuous blend using laser scanning confocal microscopy. The continuity of two components allows for the optimization of the material property by combining the desired characteristics from each component. For example, the lubricating strips in a razor blade has a continuous phase of lubricating polymer such as polyethylene oxide with another continuous phase of polyethylene or polystyrene as a mechanical support [17]. Figure 3 shows a cross section of a lubricating strip. Co-continuous structure is also used in the fabrication of conductive polymer blends in which a conductive polymer phase is supported by a mechanically robust polymer by a co-continuous phase network [18, 19]. Besides, recent research has utilized co-continuous polymer blends to extract or etch a single continuous phase to form a porous film [20-25]. For example, Trifkovic et al. has investigated the processing conditions of the co-continuous morphology of polyethylene (PE)/poly(ethylene oxide) (PEO) blends and fabricated a porous PE sheet by water extraction of PEO. The porous PE sheet can be used as a mechanical support layer for gas separations [26].

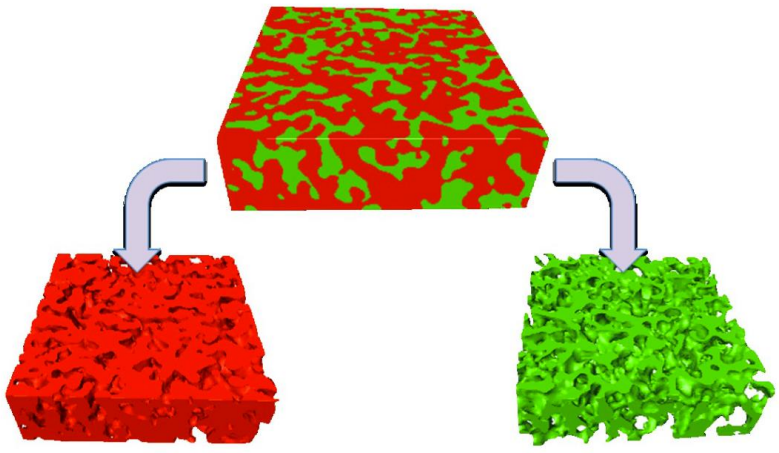

Figure 2: A 3D reconstruction of a co-continuous LDPE/PEO blend by laser scanning confocal microscopy [16]

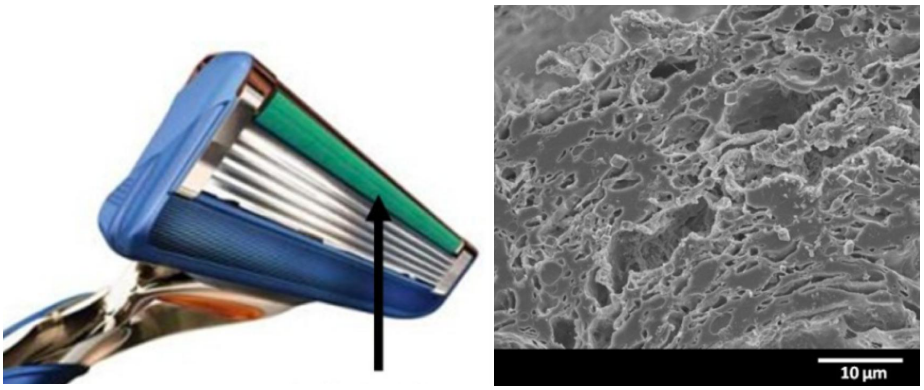

Figure 3: A SEM image of the lubricating strip in a razor blade [16]

The major difficulty is to obtain a desired co-continuous structure by mechanical mixing and maintain the optimized morphology after blends processing [27]. Because co-continuous morphologies in matrix are not in an equilibrium state under quiescent conditions and will change morphology due to the interfacial tension [28]. The thermodynamic non-equilibrium morphology of co-continuous blends causes difficulties in understanding the morphology and behavior of the material due to the phase coarsening and dispersed droplets formation in the morphology. Phase coarsening is driven by the high molecular weight and the interfacial tension that tend to minimize the interfacial areas. Traditionally, the desired co-continuous morphology is processed by quenching the non-equilibrium blends immediately to freeze the morphology. As the blends coming out of the melt compounder, it will undergo morphology changes through self-similar coarsening, filament breakup, and retraction [26].

This research utilizes an easy-to-make and low-cost method, the wax templating method, to achieve thermodynamically stable polymer blends with co-continuous morphology. This fabrication approach allows for the formation of a stable submicrometer

structure without mechanical mixing. It also provides exceptional opportunities for synthesizing new polymer blends that are inaccessible using classical blending strategies.

1.3 Fabrication of Interconnected Porous Structure by a Microsphere Templating Method

The use of an interconnected porous matrix is an effective way to obtain co-continuous phase morphology in terms of processability and stability of the morphology. This method promises a controllable generation of desired open-cell porous structure with interconnected microchannels. The specified pore size and distribution can be obtained by tuning the material and process parameters [29]. There has been a growing interest in developing interconnected porous elastomers because of its high deformability and interconnected structures. It has been majorly driven by applications in cell migration in soft tissue engineering, porous matrix, medical implants, microfluidic devices, porous substrates for catalytic reaction, and membrane filtration units with adjustable permeability [29-31]. For example, Vunjak-Novakovic et al. fabricated porous poly(glycerol sebacate) elastomer with improved mass transportation capability using a salt leaching and carbon dioxide laser piercing process [32]. Wagner et al. used a thermally induced phase separation method to produce a biodegradable porous poly(ester urethane)urea elastomer [33].

In the co-continuous polymer blends, the morphology of the porous matrix requires high controllability and interconnectivity. One general challenge in the fabrication of porous materials is the precise control of the interconnected porous structure. Common

fabrication methods such as particulate leaching and phase separation involves a large amount of toxic solvent in the preparation process, which is environmentally unfriendly and time consuming.

A microsphere-templating process was adapted in this research for creating the porous elastomer matrix. This method gives a well-defined co-continuous porous structure with interconnected microchannels. In this process, a wax microsphere template is first prepared by thermal sintering wax beads close to the wax melting temperature. The optimal sintering temperature for forming a stable three-dimensional template is approximately 4˚C below the wax peak melting temperature [31]. An example of the morphology of a sintered microsphere template is shown in Figure 4. Then low-viscosity prepolymers and catalysts of elastomer are cast into the wax template. After the elastomer is cured, the template is sacrificially removed to produce the desired co-continuous porous structure. Figure 5 shows a schematic of the fabrication process of porous elastomers [30]. There are three methods for the removal of wax template: squeezing, centrifuging, and solvent extraction. For the squeezing method, the sample is heated above the wax melting temperature and then squeeze repeatedly until the sample weight is constant. Similarly, in the centrifuging method the sample is heated above the wax melting temperature then immediately centrifuged until the sample weight becomes constant. The porous structure can also be obtained by immersing the sample into a solvent to extract out the wax template [31].

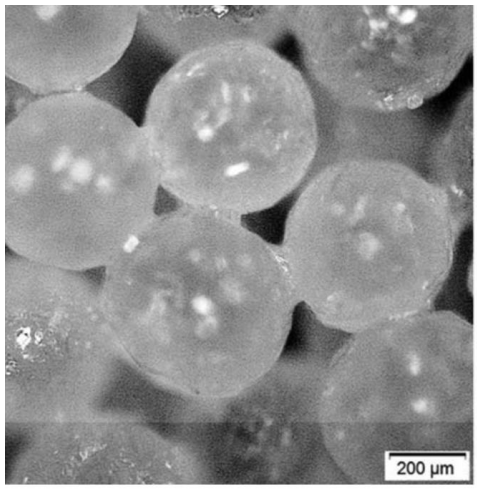

Figure 4: The morphology of a sintered microsphere template [31]

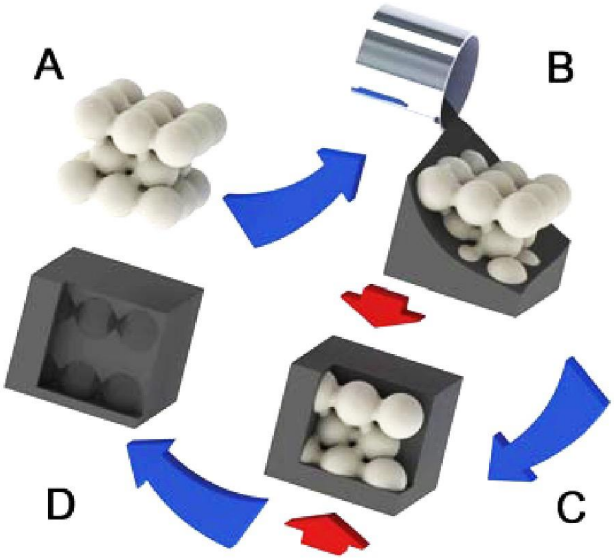

Figure 5: A schematic of the porous elastomer fabrication process [30]

From a thermodynamic point of view, the wax microsphere sintering is driven by the tendency of free energy minimization by reducing the surface area. A kinetic model for viscous sintering proposed by Eshelby is used to describe the sintering of two contacted neighboring wax beads [34]:

$$\frac{r_n}{r} = \left(\frac{t\gamma}{\eta r_0}\right)^{1/2} \quad (1)$$

where r_0 is the initial microsphere radius, r is the sintered microsphere radius, r_n is neck radius, t is sintering time, η is viscosity, and γ is surface tension. Within a narrow temperature range, the surface tension can be considered as a constant so the ratio of r_n/r is primarily determined by the sintering time t and the viscosity of the material η [31].

The mechanical properties of interconnected porous material have been investigated in recent researches. For example, Migneco et al. studied the nonlinear elastic behavior of poly(glycerol-dodecanoate) porous scaffolds and fit their data using the Ogden Model [35]. Jeong and Hollister used an exponential model to investigate the compressive stress-strain behavior of poly(1,8-octanediol-co-citrate) scaffolds with various porous density during biodegradation [36]. Mitsak et al. characterized mechanical properties of poly(glycerol sebacate) scaffold under different curing conditions and were able to fit their stress-strain data to the Neo-Hookean Model [37]. Hong et al. studied the micromechanical characteristics of the interconnected porous polysiloxane [30]. They found that the deformation of the microchannels is a highly nonaffine deformation, which means the size change of a microchannel does not follow macroscale deformations. Figure 6 shows the interconnected porous structure to illustrate this point. Under nonaffine deformation, the ratio of α' over α is not proportional to the applied stretch to the bulk material and can be affected by the channel orientation.

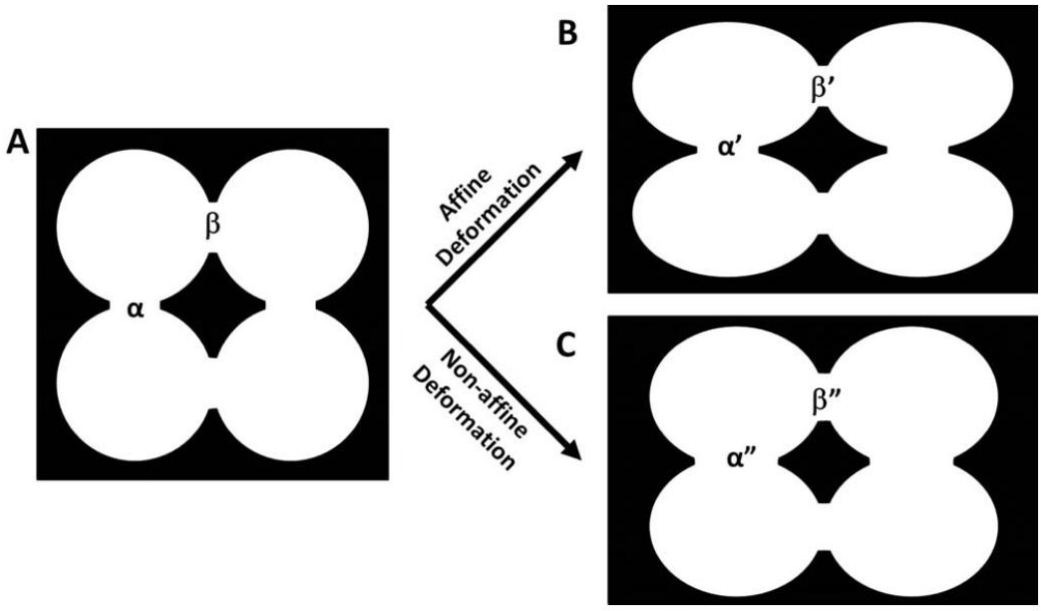

Figure 6: An illustration of affine deformation and nonaffine deformation [30]

1.4 Research Motivation and Objectives

The application of porous structure is emerging in the development of membrane permeability and functionality. Recent publications shed light on how membrane performance can be enhanced by modifying the microstructure of membranes via mechanical stretching. Early studies in neuroscience showed that mechanical stretch to neurons results in a magnitude-dependent increase in transient plasma membrane permeability [38]. Knoell et al. stated that pore aspect ratio (ratio of the lengths of the pore major axis and minor axis) of membrane influenced membrane performance in which increased pore aspect ratio results in increased water flux. However, the effect of controlled pore aspect ratio on membrane performance was not quantified in Knoell's work. Later, Morehouse et al. further investigated the effect of mechanical stretching on the aspect ratio

of pores in microporous poly(vinylidene fluoride) (PVDF) membranes along with the performance of these membranes in terms of water diffusivity [39-42]. Morehouse et al. showed that uniaxial stretching a membrane elongated pores so increased their aspect ratio of membrane. Morehouse et al. also demonstrated that by applying strain of 80% to microporous PVDF membranes pure water flux increased up to 50% over that of non-stretched membranes. However, previous work is limited to membranes with a low elastic stretchability, and the aspect ratio of the pores is not mechanically tunable once the membrane undergoes plastic deformation.

In this research, elastomer is selected and fabricated into a porous structure because it can provide mechanical support and capable of sustaining large elastic strains. The pore shape change and recovery can be simply in situ adjusted by mechanical stretching of the bulk elastomer. However, the use of elastomers in membrane filtration applications is limited by their low water permeability and the porous structure does not allow for molecular selectivity. For example, experimental results in this research show that a 100um thickness 20:1 PDMS membrane can be biaxially stretched at least twice its original length but its water permeability is only $6\times10^{-13}m^2/s$. This functionality limitation can be accommodated by filling hydrogels into the co-continuous porous structure. Hydrogels have a crosslinked polymeric network with a high water permeability but low stretchability. For example, experimental results in this research show that the water permeability of a PEG-HEA hydrogel is 18.26 $\frac{L*um}{m^2*hr*bar}$ but the hydrogel fractures at a strain of 0.15 under a compressive load. In hydrogels, the polymer chains in the crosslinked network can function as a molecular sieve that only allows small molecules to diffuse through. Thus, the motivation of this research is to fabricate an elastomer-hydrogel composite that

combines the high stretchability of elastomer and high water permeability and salt diffusivity of hydrogel for membrane filtration applications.

The primary objective of this research is to design, fabricate, and characterize a stretchable, water permeable elastomer-hydrogel composite material that can be used as a mechanically tunable sieve in drug delivery and biomedical applications. The composite material is synthesized by filling a co-continuous porous elastomer with hydrogels in order to combine the high deformability of elastomers and the high water permeability of hydrogels. Polydimethylsiloxane (PDMS) is chosen as the elastomeric matrix because of its biocompatibility and high stretchability. Polyacrylamide hydrogels are cast into the porous PDMS to function as an intermediate for molecule implant and diffusion. To improve the compatibility between PDMS and hydrogels, the poly(dimethylsiloxane-ethylene oxide polymeric) (PDMS-b-PEO) is used as a surfactant additive to add into PDMS for improving the hydrophilicity of PDMS. The mechanical behavior such as stiffness and swelling ratio of the elastomer-hydrogel composite were characterized. The diffusion properties such as salt diffusivity is also tested and analyzed.

1.5 Thesis Outline

In this research thesis, Chapter 1 gives an introduction to the fundamentals of polymer blends with a focus on co-continuous structure polymer blends. This chapter also discusses a novel fabrication method of interconnected porous structure, microsphere templating process, that allows for good processability and stability of co-continuous structure, which leads to the motivation and the objectives of this research. Chapter 2 presents the

fabrication and characterization of a hydrophilic PEO-PDMS composite that is used as interconnected porous matrix in co-continuous structure polymer blends. This chapter also discusses the fabrication and characterization of interconnected porous PEO-PDMS by the microsphere-templating process. Chapter 3 introduces the fabrication and characterization of hydrogels that are filled in the interconnected pores of the co-continuous polymer blends. Chapter 4 presented the fabrication and characterization of PDMS-hydrogel composite. The strain field in the hydrogel domain is also analyzed using a finite element analysis model. Chapter 5 gives a summary of the research work, and the findings, limitations and future works are discussed.

Chapter 2

Fabrication and Characterization of Interconnected Porous PEO-PDMS

In this research, PDMS is selected as the matrix elastomer in the proposed elastomer-hydrogel composite to provide mechanical support with a high stretchability. This chapter focuses on the fabrication and characterization of PDMS, along with hydrophilicity enhanced PEO-PDMS. The hydrophilic PEO-PDMS allows water to fast flow into the microchannels of the porous PEO-PDMS matrix. The intrinsic material behavior of PDMS and PEO-PDMS is characterized, including biaxial stretchability test, water permeability test, contact angle test, DMA tests, indentation test, and fracture energy test. This chapter also discusses the fabrication of interconnected porous PEO-PDMS using microsphere templating process and its stress-strain behavior is also studied and analyzed.

2.1 PDMS Sample Preparation

In this research, Polydimethysiloxane (PDMS) is selected to be the elastomeric matrix in the co-continuous polymer blends. This nontoxic material has a high deformability, along with high thermal and chemical stability. PDMS has a molecular structure in which an inorganic silicone-oxygen backbone chain with organic side groups attached to silicon atoms. Figure 7 shows the molecular structure of a silicone polymer chain.

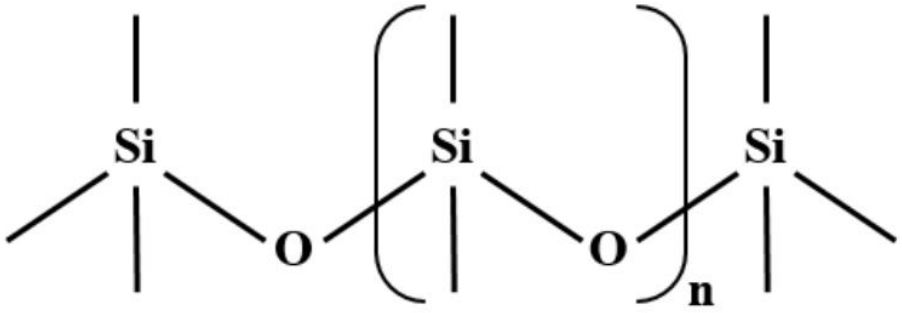

Figure 7: Molecular structure of a silicone polymer chain [43]

PDMS prepolymer is prepared by mixing the silicone base (Sylgard® -184) and the curing agent (cross-linker) from Dow Corning Corp. Table 1 shows some typical properties of PDMS. The ratio of the silicone base to the curing agent determines the stiffness and toughness of the cured PDMS. After that, the prepolymer mixture was well stirred by hand using a fork for 5 minutes then placed in a vacuum desiccator to degas for one hour until all the air bubbles in the mixture were expelled. The prepolymer is in a low-viscous liquid state which is beneficial to processing such as molding and casting. The prepolymer was then cured at 40˚C for 72 hours and became solid-state.

Table 1: Typical properties of PDMS [44]

Color	Viscosity (Mixed)	Density (Cured)	Cure Time at 25˚C*	Tensile Strength*
Colorless	3.5 Pa-sec	1.03g/cm^3	48 hours	6.7 MPa

* Base to agent weight ratio is 10:1

2.2 Characterization of PDMS

2.2.1 Biaxial Stretchability Test of PDMS

In this section, the biaxial stretchability of PDMS is characterized by measuring membrane central deflection at various differential pressure conditions. As an increasing differential pressure is applied to a circular shaped PDMS film, the film deflects into a blister configuration and exhibits biaxial stretching. A schematic of a deflected film is shown in Figure 8. Assuming the film deflection is much greater than the film thickness and membrane is in a circular shape, the film deflection at different applied pressures can be calculated by:

$$w_0 = 0.662a \sqrt[3]{\frac{pa}{Et}} \tag{2}$$

where p is the applied pressure on the membrane, E is the Young's modulus of the membrane, t is the membrane thickness, a is the radius of the circular membrane.

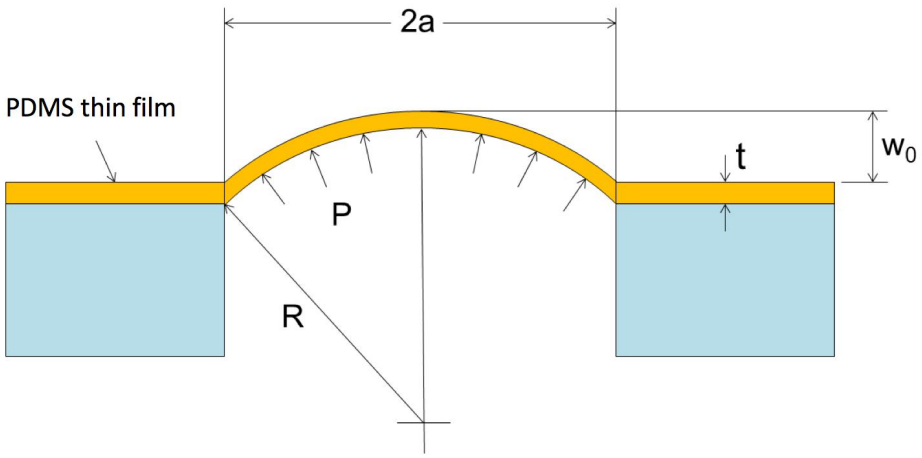

Figure 8: A schematic of a deflected film under differential pressure

The testing setup for the film deflection test is shown in Figure 9. The setup consists of three main components: a pressure calibrator, a syringe pump, and a modular micro-tribometer from Materials Tribology Lab at University of Illinois. A 100 μm thickness circular shaped (d=3mm) PDMS membrane with a crosslinking ratio of 20:1 was clamped by two steel plates. The Young's modulus of 20:1 PDMS is 308 kPa. In this test, the membrane deflection was measured at pressures ranging from 1 kPa to 38 kPa in steps of 1 kPa. A constant pressure was applied using a 10ml syringe where the syringe was connected to the chamber through a tee connector. A NE1000 syringe pump from New Era Pump System Inc. was employed to apply a constant pressure to the film, and the applied pressure was measured using a pressure calibrator from Fluke Corporation. The syringe pump allowed for a relatively constant pressure applied to the blister throughout the testing process. An indenter was utilized to measure the deflection at the center of the blister at different pressures.

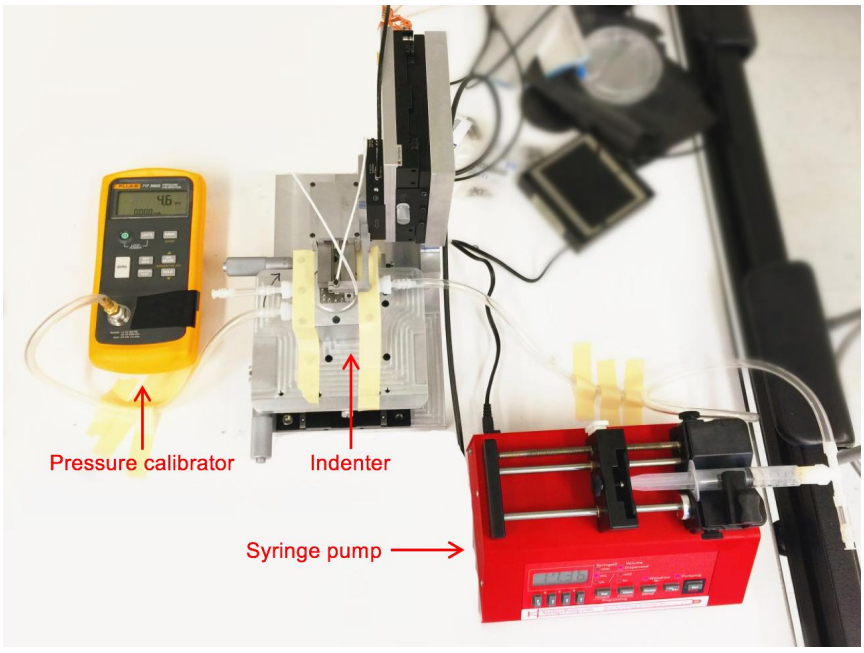

Figure 9: Testing setup for membrane deflection characterization tests

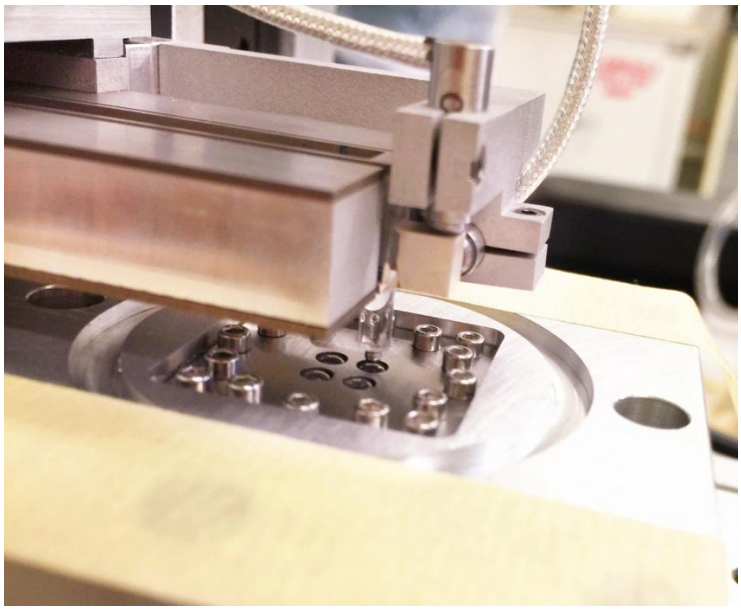

Figure 9 (cont.): Testing setup for membrane deflection characterization tests

Figure 10 shows the blister configurations at various differential pressures. The experimental results are shown in Figure 11. For (P/E) between 0.06 and 0.04 the deflection increasing rate becomes higher. This is because the steel plates that clamp the PDMS film constrained the expansion of the blister and formed a neck in the bulging blister due to the thickness of the steel plates. In summary, PDMS shows a high stretchability and can be biaxially stretched at least twice its original length.

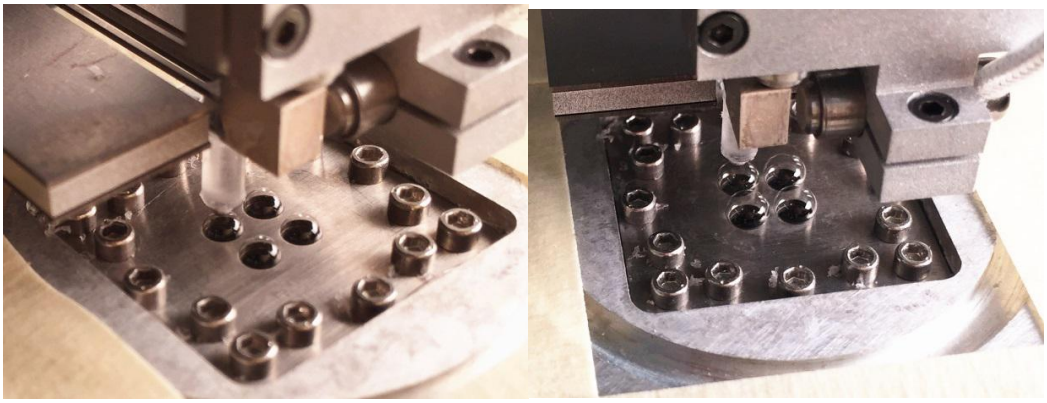

Figure 10: Blister configurations at various differential pressures

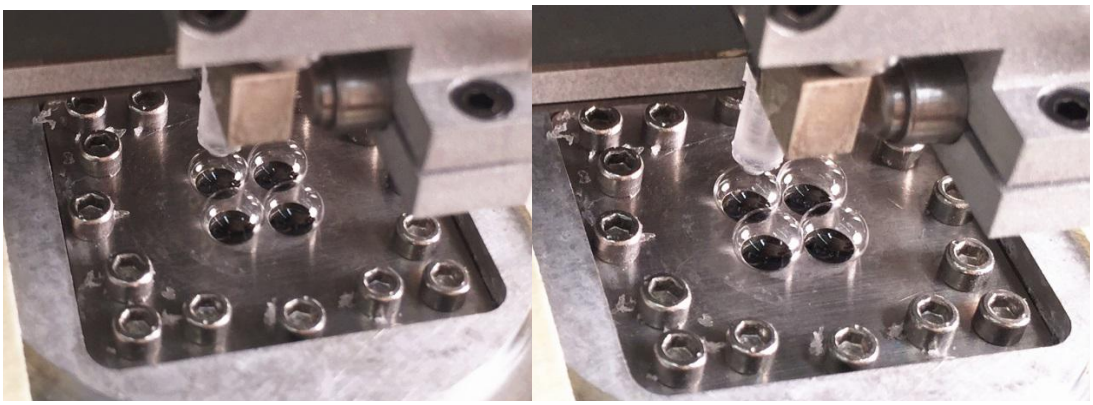

Figure 10 (cont.): Blister configurations at various differential pressures

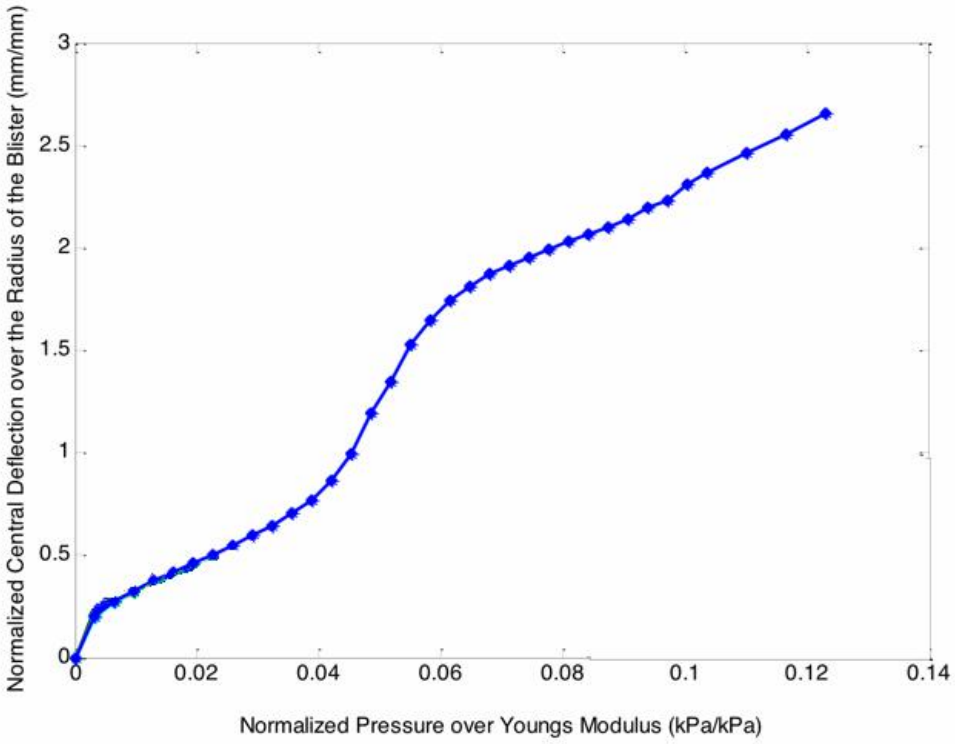

Figure 11: Film central deflection at various differential pressures

2.2.2 Water Permeability Test of PDMS

This section discusses the characterization of water permeability of PDMS using an osmotically driven membrane processes. Forward osmosis is an osmotically driven

membrane process in which water diffuses across a membrane driven by a difference in osmotic pressure across the membrane. Forward osmosis, therefore, does not require an applied hydraulic pressure as a driving force like the reverse osmosis process. Osmotic pressure in forward osmosis can be significantly greater than hydraulic pressure in reverse osmosis, potentially leading to higher water diffusion flux. Figure 12 shows the schematic diagram of the apparatus for water permeability test. The actual experimental setup is shown in Figure 13. The apparatus consists of three main components: a feed water chamber (FC), a draw solution chamber (DC), and a PDMS film placed in between. The working principle of this measurement is based on an osmosis-driven water flow from FC to DC through a PDMS thin film. The film has an effective area of 0.28 cm^2 with a thickness of 100 μm. The driving osmotic potential is provided by the difference of the solution concentration between the two chambers. 1M NaCl was used as an osmolyte in this test. A recirculation pump was connected to each chamber to circulate the flow with a flow rate of 20 ml/min in order to minimize the concentration polarization effects during the testing process. A pressure sensor was mounted to the chamber to monitor the differential pressure in the two chambers. A valve was mounted to the lower position of each chamber to control the flow and to drain out the water/solution in the chamber after the test. A conductivity probe was used to monitor the reverse salt diffusion into FC. Each chamber was connected to a sealed flask which was used for measuring the weight change throughout the testing process. Water flux across the membrane was determined by measuring the weight change of the solution in the flask over a period of time thus the water permeability can be calculated.

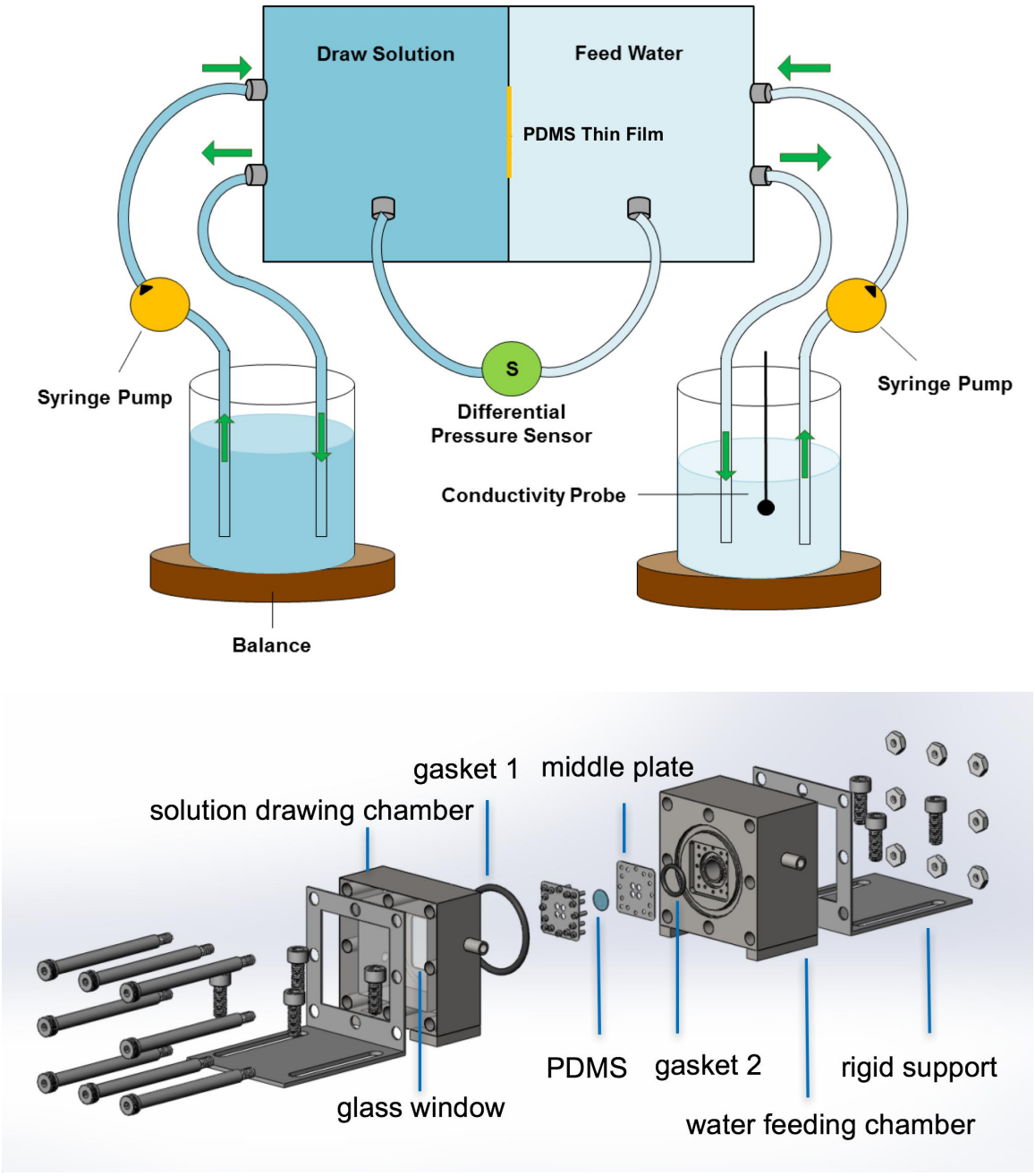

Figure 12: Schematic diagram of the water permeability test setup

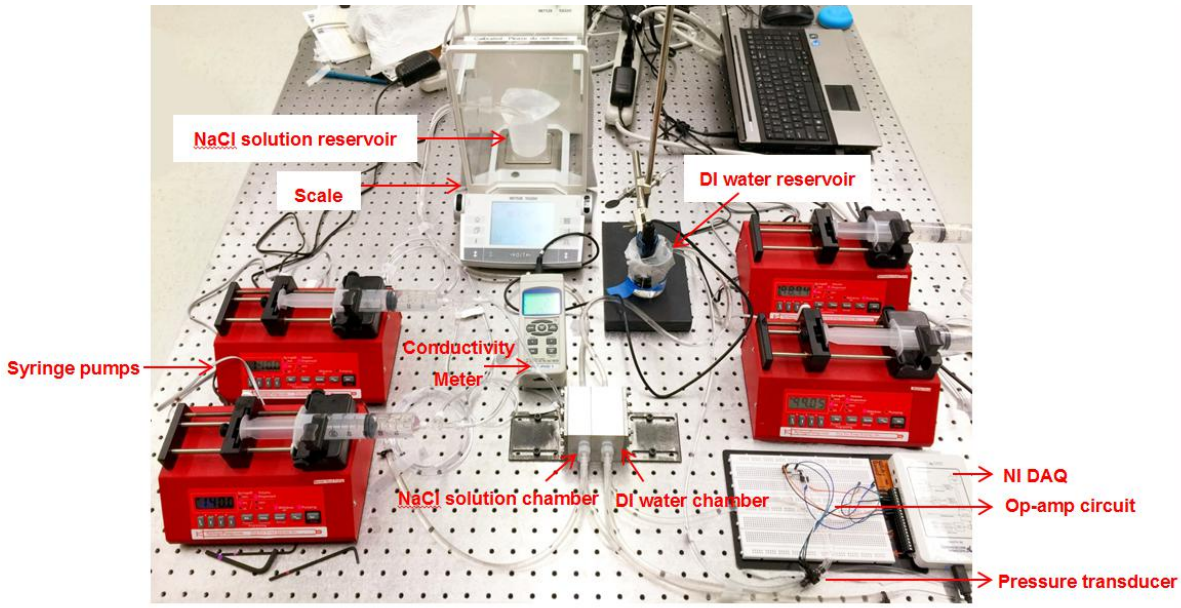

Figure 13: Experimental setup for water permeability test

Figure 14 shows the mass change in the draw solution chamber over time. It can be seen that the mass change in the draw solution chamber is decreasing over time. The result indicates the low water permeability of PDMS and the weight decrease is mainly caused by the water evaporation in the system over time.

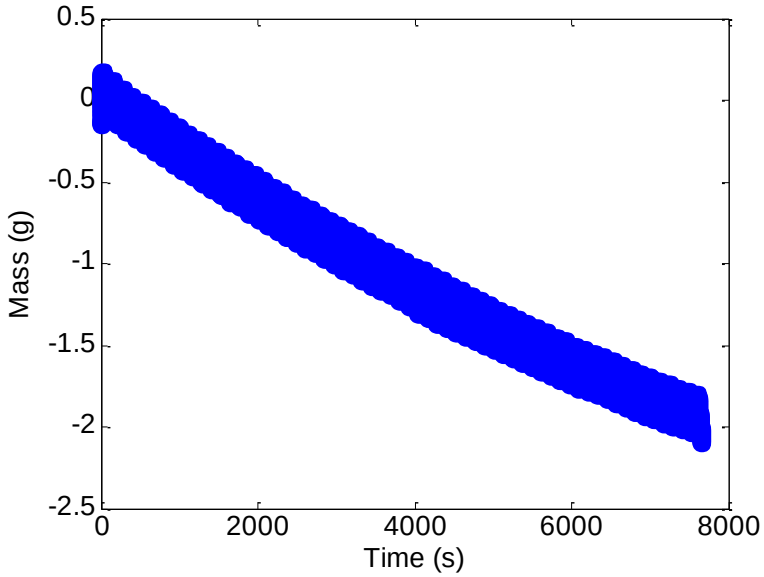

Figure 14: Mass change in the draw solution chamber in water permeability test

2.3 Hydrophilic PEO-PDMS Fabrication

The hydrophobicity of PDMS is unfavorable in the fabrication of PDMS-hydrogel co-continuous polymer blends because the hydrogel solution may not be easily cast and flow into the microchannels of the porous PDMS matrix. One common approach for modifying the hydrophilicity of PDMS is its exposure to oxygen plasma. However, the plasma treatments only change the surface properties and the hydrophilicity lasts only a few hours [45]. To improve the hydrophilicity of PDMS, this research uses block copolymer poly(dimethylsiloxane-ethylene oxide polymeric) (PDMS-b-PEO) as a surfactant additive to add into the PDMS prepolymer mixture to improve the hydrophilicity of PEO-PDMS. The chain segment length of PDMS-b-PEO are varied to tune the hydrophilicity properties. The molecular structure of PDMS-b-PEO is shown in Figure 15. The additive PDMS-b-PEO comprises a hydrophobic segment that is compatible with PDMS and allows the additive to be solubilized and to anchor the additive in the cured PDMS. On the other hand, the hydrophilic pendant chain in the additive gives desirable surface hydrophilic properties to the elastomer [46].

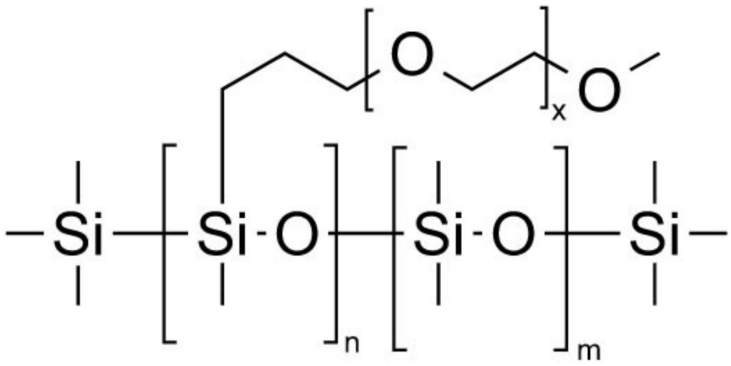

Figure 15: The molecular structure of the poly(dimethylsiloxane-ethylene oxide polymeric) [47]

In this experiment, the additives PDMS-b-PEO are purchased from Polysciences Inc. Some properties of PDMS-b-PEO are shown in Table 2. The extent of hydrophilicity of PDMS can be tuned by the weight ratio of PDMS-b-PEO to PDMS prepolymers. On the other hand, as the weight percent of PDMS-b-PEO increases, the sample becomes milky and the viscosity of the mixture increases, which is difficult for degassing in the preparation process. Figure 16 shows an image of the comparison of 10:1 PDMS, 10:1 PDMS with 1% PDMS-b-PEO addition, and 10:1 PDMS with 5% PDMS-b-PEO addition.

Table 2: Typical properties of PDMS-b-PEO [47]

Color	Molecular Weight	Viscosity	Density
Colorless	600 g/mol	0.02 Pa*s	1.07 g/cm^3

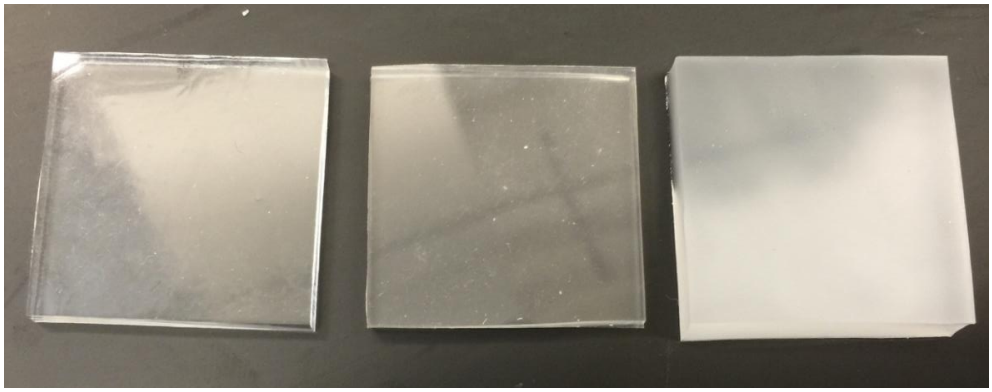

Figure 16: 10:1 PDMS (left), 10:1 PDMS with 1% PDMS-b-PEO addition (middle), and 10:1 PDMS with 5% PDMS-b-PEO addition (right)

In this research, the PEO-PDMS sample was prepared by adding a weight ratio of 1% to the PDMS prepolymer mixture then stirred for 15 minutes using a digital vortex mixer from Fisher Scientific Inc. The mixture was then degassed in a vacuum for one hour and carefully poured into an acrylic mold to form a thin film, as shown in Figure 18. The sample mold has a size of 30mm x 30mm x 1.6mm. The sample mold was then put into an oven for curing at 40˚C for 72 hours. After that, the cured PEO-PDMS was peeled from the mold. The surface of a PDMS-PEO sample was observed under a scanning electron microscope (SEM) from Phenom-World Inc., as shown in Figure 17. In the SEM image, the black dots are the pendant chains that provide surface hydrophilic properties of the elastomer.

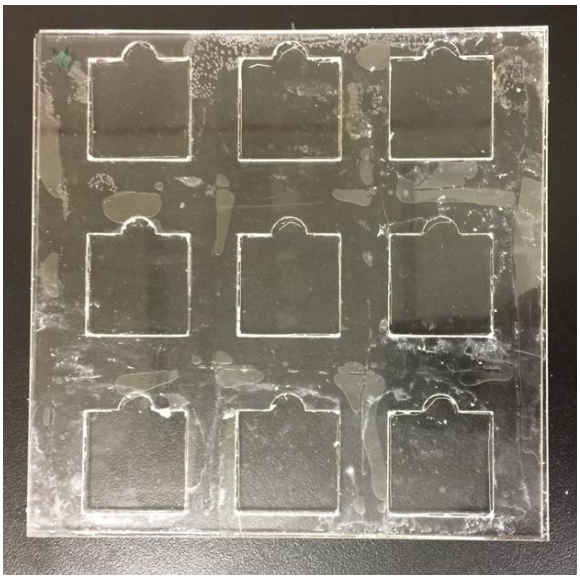

Figure 17: Acrylic mold for making thin film samples

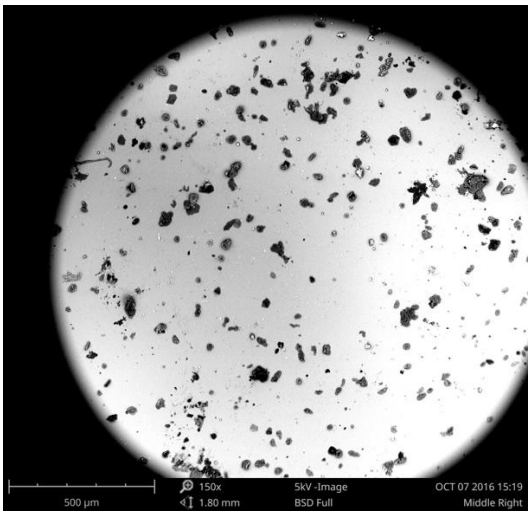

Figure 18: SEM image showing the surface of PEO-PDMS

2.4 Characterization of PEO-PDMS

2.4.1 Contact Angle Test

The hydrophilic PEO-PDMS was prepared by adding 1% weight percent of PDMS-b-PEO block copolymer to the PDMS prepolymer mixture. Due to the tethered PEO block copolymer, the surface of PEO-PDMS exhibits rapid changing wettability characteristics. A time-dependent contact angle analysis was conducted to determine surface wettability properties of PEO-PDMS. Theoretically, in the contact angle analysis the thermodynamic equilibrium of the solid phase, the liquid phase, and the gas phase is described by Young-Laplace equation [48]:

$$\gamma_{SG} - \gamma_{SL} - \gamma_{LG} cos\theta_c = 0 \quad (3)$$

where γ_{SG} is the solid-gas interfacial energy, γ_{SL} is the solid-liquid interfacial energy, γ_{LG} is the liquid-gas interfacial energy, and θ_c is the equilibrium contact angle [48]. Figure 19

shows a schematic of a liquid drop on a material surface showing the quantities in Young-Laplace equation.

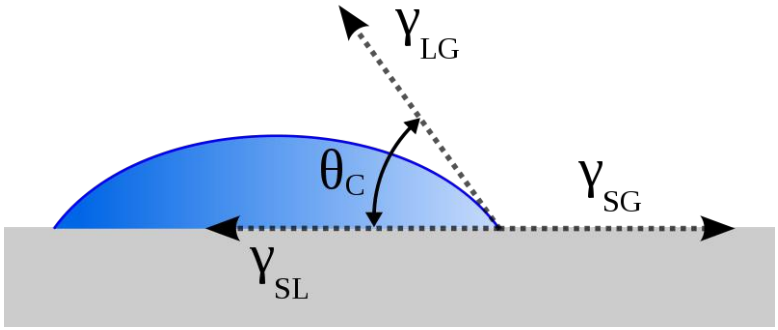

Figure 19: Schematic of a liquid drop on a material surface [51]

The contact angle measurement was carried out using a goniometer setup in the Energy Transport Lab at University of Illinois. A droplet of DI water of 2 μL was dispensed on the surface of a PEO-PDMS sample, and the contact angle was measured for 48 seconds with a frame rate of one image/sec. Figure 21 shows an image of a droplet on a PDMS surface and on a PEO-PDMS surface. Figure 22 shows the time-dependent contact angle analysis curves. In general, the contact angle of PEO-PDMS is lower than PDMS. At the same time interval, a lower water contact angle suggests higher surface hydrophilicity of the material. The high time-dependent decrease in the contact angle of PEO-PDMS is primarily attributed to the absorption and reorientation of hydrophilic PEO to the interface of polymer and water to reduce interfacial free energy [46, 49].

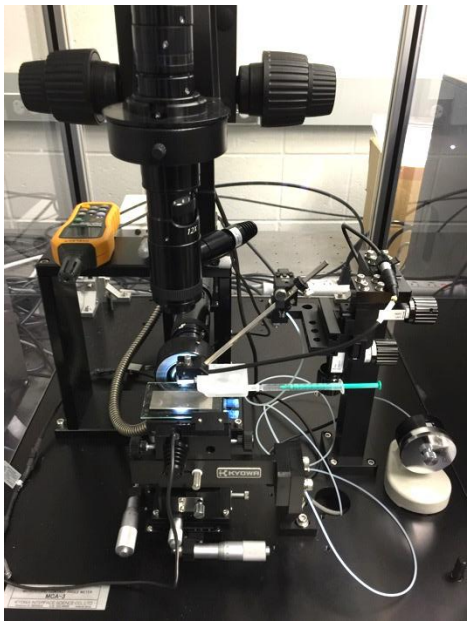

Figure 20: Experimental setup for the contact angle test (the setup is from Energy Transport Lab at University of Illinois at Urbana-Champaign)

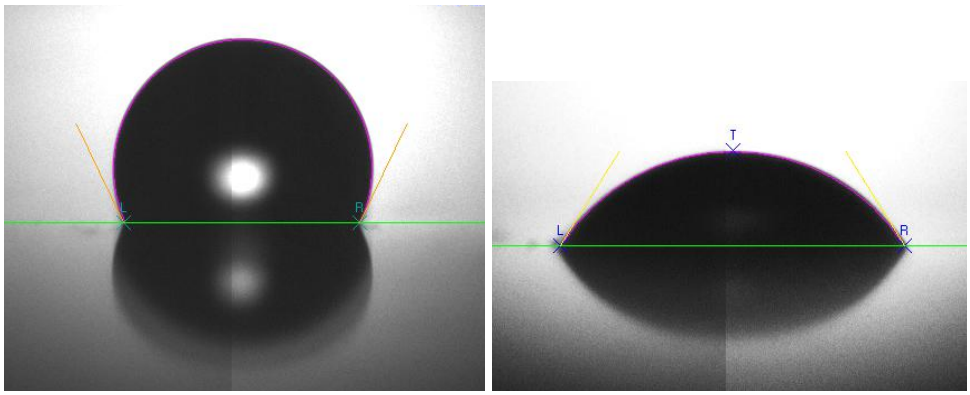

Figure 21: An image of a DI water droplet on a PDMS surface (left) and on a PEO-PDMS surface (right)

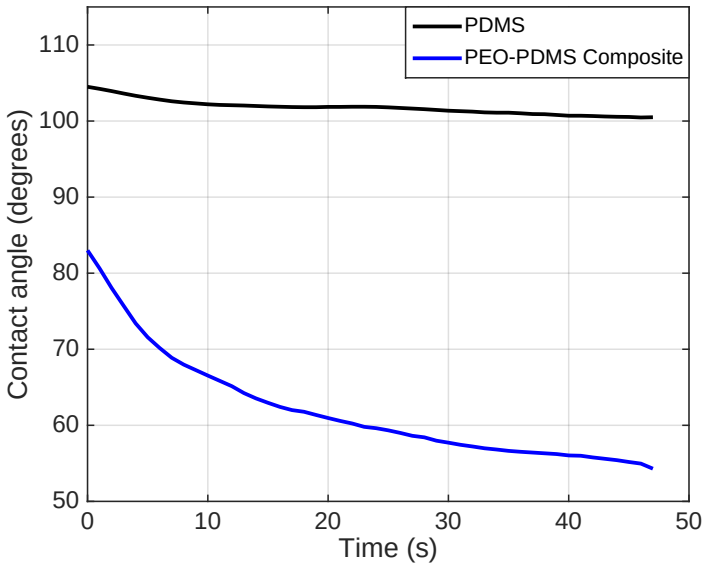

Figure 22: Contact angle analysis of PDMS and PEO-PDMS

2.4.2 DMA Tests: Strain Sweep, Creep, and Stress Relaxation

The hydrophilicity of PDMS is greatly improved by adding a block copolymer PDMS-b-PEO, but the effect of the surfactant additive to the mechanical properties of PDMS needs to be further investigated. In this section, strain sweep, creep, and stress relaxation tests were conducted using Dynamic Mechanical Analysis (DMA) to characterize the viscoelastic behavior of PEO-PDMS. DMA is a technique to measure the dynamic mechanical properties. In DMA, the complex modulus E* can be calculated by stress over strain. Since polymers behaves both like an elastic solid and a viscous fluid, the storage modulus E' and the loss modulus E" were analyzed. The storage modulus is the elastic component which relates to the stiffness of the material. The loss modulus E" is the viscous component which relates to the ability of mechanical energy dissipation by molecular

motion. E*, E', and E" are related by the tangent of phase difference δ, as shown in Figure 23. The phase difference δ can be determined by the phase lag between an input stress signal and an output strain signal.

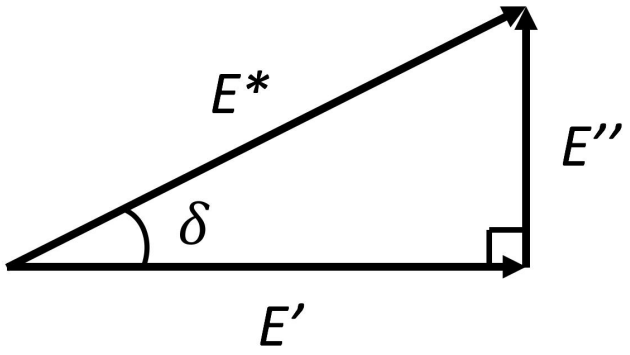

Figure 23: The relationship between E*, E', and E"

A polymeric material has time dependent properties, which means the properties depend on the strain rate and amplitude. A polymeric material must be within the linear viscoelastic region to be independent of the magnitude of deformation. The linear viscoelastic region can be measured using a strain sweep test. As a general rule of thumb, the end of the linear region is to find the strain at which the initial value of the storage modulus changes by 5% [50]. All the DMA tests in this research were carried out using Q800 DMA in the Frederick Seitz Materials Research Laboratory Central Research Facilities, University of Illinois. In the strain sweep test, the PEO-PDMS sample has a size of 9.26 mm in length, 6.64 mm in width, and 1.31 mm in thickness; PDMS is 8.61 mm in length, 6.6 mm in width, and 1.68 mm in thickness. The frequency of the test was fixed at 1 Hz and the amplitude was increased with an increment of 100 um. The results of strain

sweep tests are shown in Figure 24. It can be seen in the figure that the strain limit of linear viscoelastic region for PEO-PDMS is less than 2.7%, and less than 2.9% for PDMS.

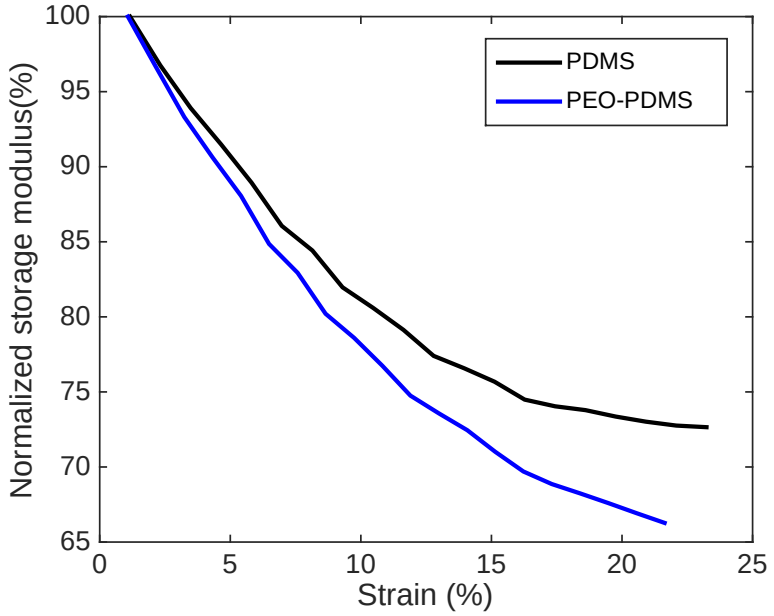

Figure 24: Strain sweep test results of PEO-PDMS and PDMS: normalized storage modulus vs. strain

The creep test was performed by applying a constant stress to a material and holding the stress for a period of time and then removing the load. The material exhibits an instantaneous elastic strain when the stress is applied, followed by an increasing strain over time due to the chain mobility. The strain change becomes slow over time. When the applied stress is removed, the elastic strain is immediately recovered followed with a time dependent strain recovery called anelastic recovery. A permanent strain may eventually be left in the material [51]. In this test, a constant stress of 16 kPa was applied to a PEO-PDMS sample and held constant for 30 minutes then removed. Figure 25 shows the creep

test results. It can be found from the figure that no major difference in the creep behavior of PEO-PDMS and PDMS.

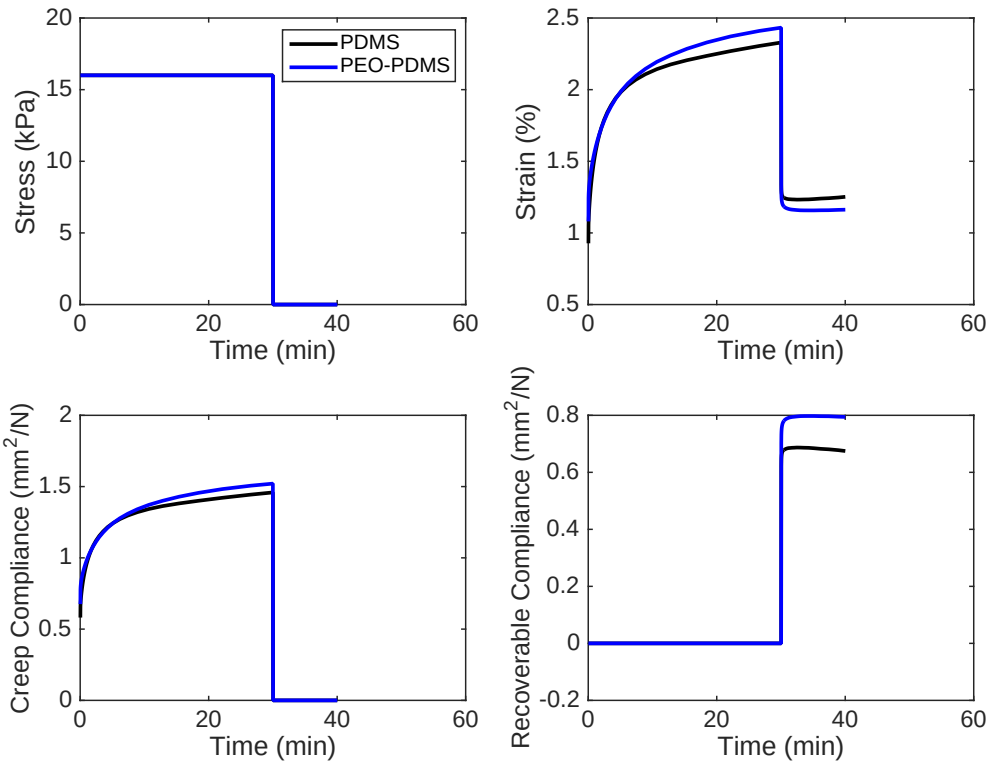

Figure 25: Creep test results of PEO-PDMS and PDMS: stress, strain, creep compliance, and recoverable compliance vs. time

The stress relaxation test was conducted by applying a constant strain to a material and holding the strain for some length of time. At a constant strain, the required stress for holding the material decreases over time due to the rearrangement of the polymer chains. In this test, a constant strain of 1% was applied to the samples and held for 30 minutes. The stress relaxation test results are shown in Figure 26. The overall stress relaxation behavior is very similar for PEO-PDMS and PDMS.

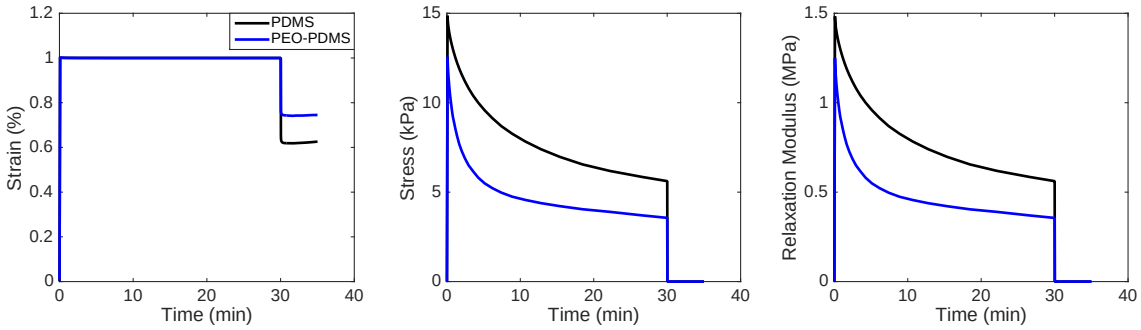

Figure 26: Stress relaxation test results of PEO-PDMS and PDMS: strain, stress, relaxation modulus vs. time

2.4.3 DMA Tensile Test

The stiffness of PEO-PDMS and PDMS was measured by a DMA tensile test. A pre-load of 0.001N was applied to the sample then an increasing tensile load was applied on the sample with a loading rate of 3N/min until 18N (load limit of DMA) was reached. Two tests were performed for each sample to validate the repeatability of the results. Figure 27 shows the stress-strain behavior of PEO-PDMS and PDMS. Elastic modulus was calculated by linear fitting stress-strain data for strain less than 2%. Table 3 summarizes the tests results. The elastic modulus of PEO-PDMS is 1.37 MPa and PDMS is 1.56 MPa. That is, the addition of PDMS-b-PEO surfactant additive results in 12.18% decrease in the stiffness of 10:1 PDMS. In general, the addition of PDMS-b-PEO does not affect much on the stiffness of PDMS.

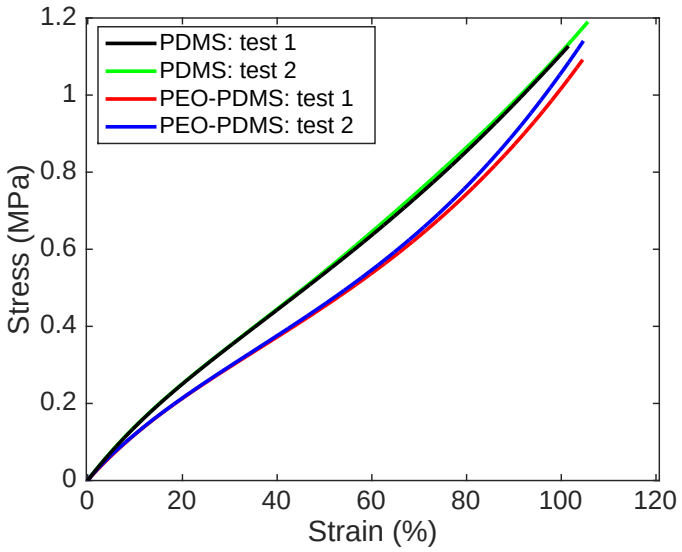

Figure 27: The stress-strain curve of PEO-PDMS and PDMS

Table 3: Elastic modulus test results of PEO-PDMS and PDMS by DMA tensile tests

Elastic Modulus (Unit: MPa)	PEO-PDMS	10:1 PDMS
Test 1	1.34	1.55
Test 2	1.40	1.57
Mean	1.37	1.56
Relative error	2.19%	0.64%

2.4.4 Indentation Test

Recently, indentation technique has been demonstrated as a simple and quick approach to characterize the elastic modulus of a material. The elastic modulus can be determined from the indentation load and the corresponding displacement measurements. The

displacement measurement is facilitated using a high-resolution equipment at a scale of micrometers or nanometers [52]. This testing method is of particular interests to the characterization of soft materials because of its high precision at small scales. In this research, an indentation test was conducted to measure the elastic modulus of PEO-PDMS then compared to the results from the tensile tests for validation. The basic principle of an indentation test is to indent a sample surface with a spherical probe to a specified depth and measure the load-displacement response in the loading process. The load-displacement data is then fit to the Hertzian model to calculate the elastic modulus of a material. Figure 28 shows a schematic of the contact surface in the Hertzian model.

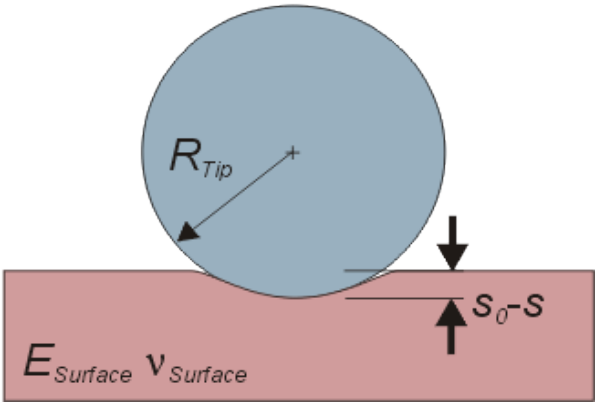

Figure 28: A schematic of the contact surface in Hertzian model [53]

Using the Hertzian contact model, the elastic modulus of a material can be calculated by the following equation:

$$E_{surface} = \frac{3F(1-v^2)}{4\sqrt{R_{tip}}(s_0 - s)^{3/2}} \quad (4)$$

where $E_{surface}$ is the elastic modulus of the sample, F is the applied force, v is the Poisson's ratio of the sample, R_{tip} is the radius of the spherical tip, $(s_0 - s)$ is the

indentation depth. There are four assumptions for the application of Hertzian contact model: 1) The stiffness of the sample is much less than that of the probe. 2) The indentation depth is far less than the radius of the probe. 3) No adhesion on the contact surface of the tip. 4) No viscoelasticity during indenting process.

A modular micro-tribometer from Materials Tribology Lab at University of Illinois was used for the indentation tests. Figure 29 shows the experimental setup for the indentation test of PEO-PDMS. The indenter has a spherical shaped steel tip with a radius of 1mm. The PEO-PDMS sample has a non-adhesive flat surface with a thickness of 2.5cm. The probe was indented onto the sample surface until it reached 10mN, and the corresponding indentation depth is 25μm. The loading process was in two seconds to minimize the effect of viscoelasticity. Figure 30 shows the fitting of the load-displacement data from the indentation test to the Hertzian model. The R^2 value of the curve fitting is over 99.85%.

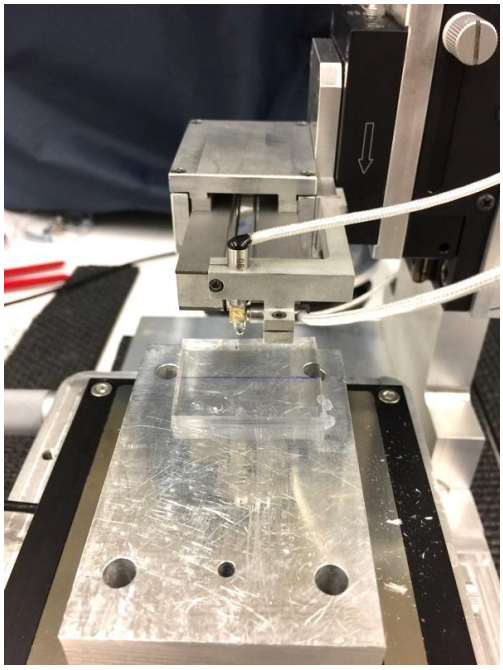

Figure 29: Experimental setup for indentation tests

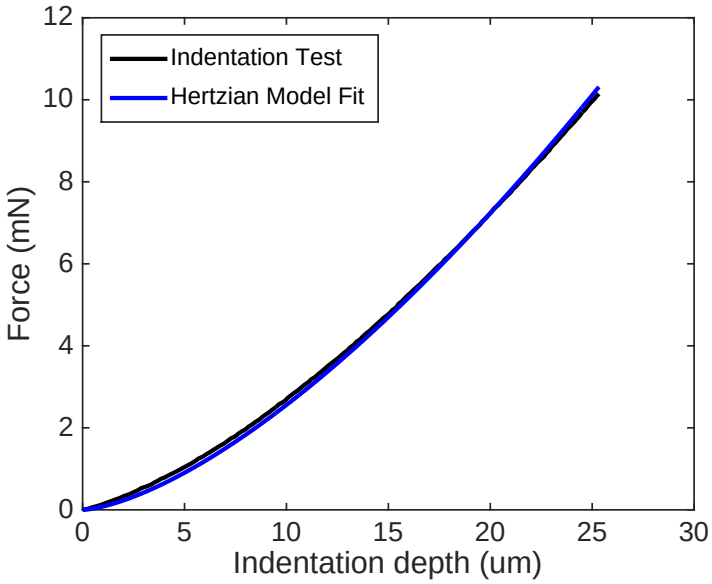

Figure 30: Curve fitting of force-displacement data from indentation tests to the Hertzian model

Assuming the Poisson's ratio of PEO-PDMS is 0.5, the best fit of the experimental data to the Hertzian model outputs the elastic modulus. The results are summarized in Table 4 and 5. From the indentation test results, the elastic modulus of PEO-PDMS is 1.445MPa, which is slightly higher than the modulus measured by DMA tensile test 1.37MPa. The relative error of the modulus test by the two test methods is 5.19%.

Table 4: Indentation test results of PEO-PDMS

Test	Elastic Modulus (MPa)	The R^2 value
Test 1	1.44	99.88%
Test 2	1.45	99.85%

Table 5: Test result comparison of PEO-PDMS by DMA tensile tests and indentation tests

Testing method	Elastic Modulus (MPa)	Relative error
DMA – Tensile test	1.37	5.19%
Indentation test	1.445	

2.4.5 Fracture Energy Test

The fracture energy is an important intrinsic material property of a highly stretchable material, which describes the resistance of a material to the propagation of an existing crack. This section discusses the fracture energy tests of PDMS and PEO-PDMS using the tearing test method. In the tearing test method, two rectangular PEO-PDMS samples with the same material and geometry were prepared, one unnotched sample and one notched sample with a crack length of 15mm. The notched sample was first clamped between two clamps using a test stand from Mark-10 (ESM301) then an axial tensile stress was applied until it reached a critical displacement in which the notch in the sample started to propagate into a running crack. After that, the unnotched sample was also stretched to the critical displacement so the area under the stress-displacement curve of the unnotched sample is the fracture energy per unit area, which gives the absorbed strain energy per unit cross-sectional area before the crack propagation. Figure 31 shows a schematic of the configurations and principles of fracture energy calculation. Figure 32 shows the experimental setup and the crack propagation of the cracked sample.

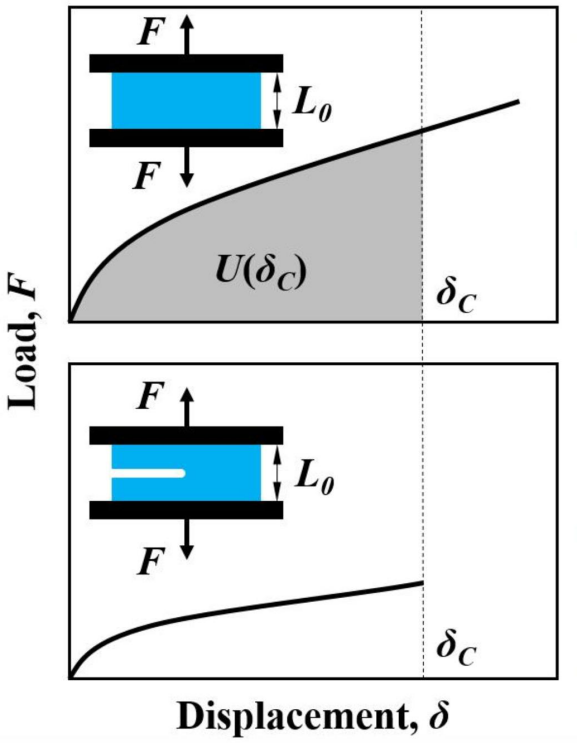

Figure 31: The configurations of unnotched and notched sample and their load-displacement responses [43]

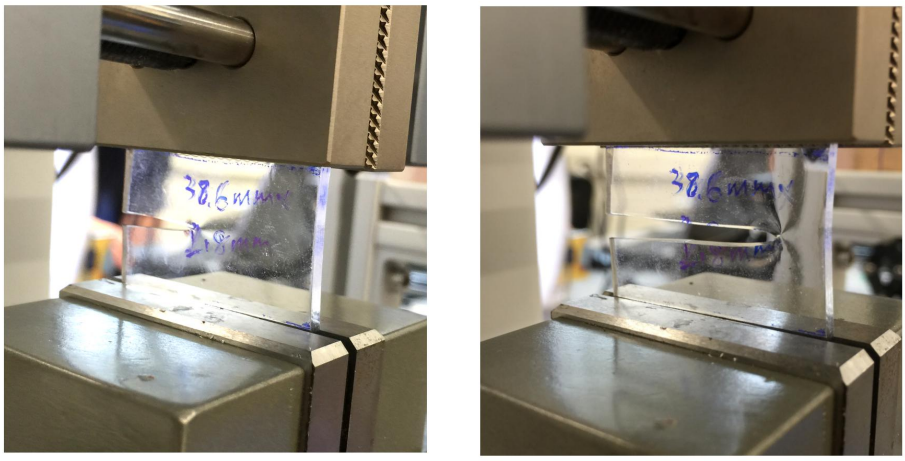

Figure 32: Notched sample before crack propagation (left) and after crack propagation (right)

Fracture energy of both PDMS and PEO-PDMS was tested and analyzed. Figure 33 shows the load-displacement curves in the fracture energy tests. Two tests were conducted for each sample and the corresponding fracture energy is summarized in Table 6. The fracture energy of PEO-PDMS is 332.7 J/m^2 and of PDMS is 304.63 J/m^2, which indicates that the addition of the surfactant PDMS-b-PEO does not impact much on the fracture energy of PDMS.

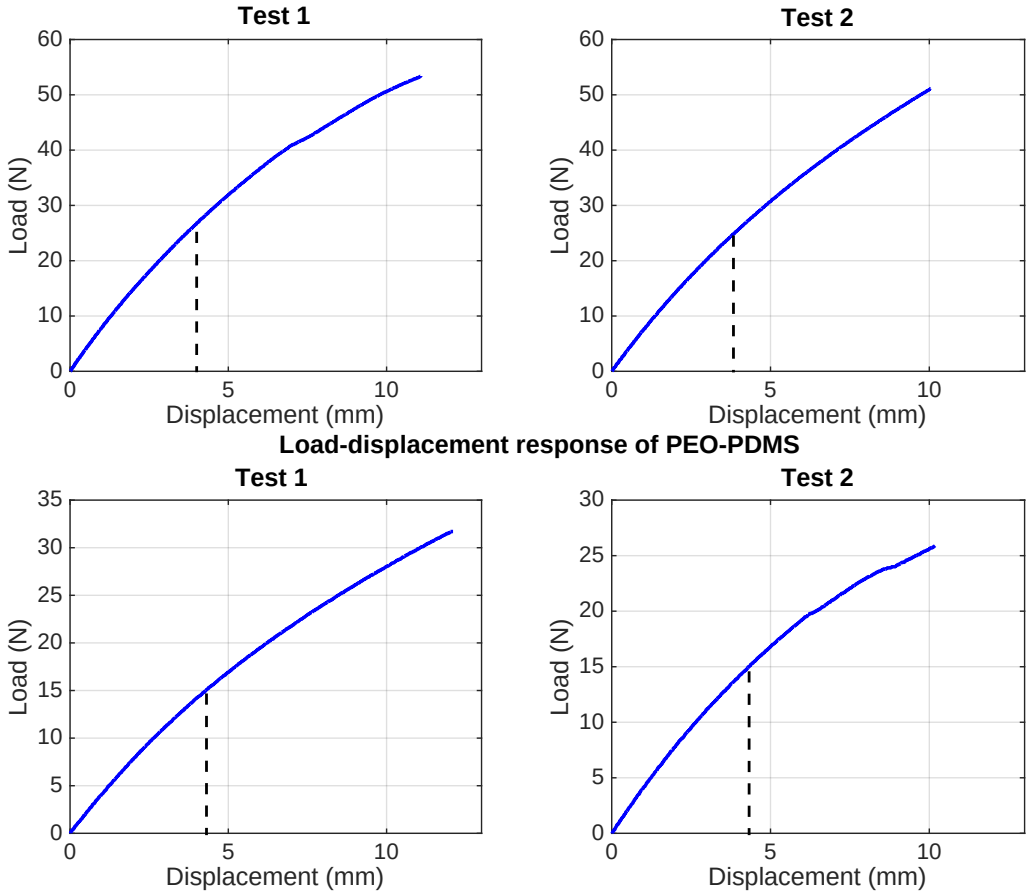

Figure 33: Load-displacement response of PEO-PDMS and PDMS in fracture energy tests

Table 6: Fracture energy test results of PDMS and PEO-PDMS (unit: J/m^2)

Sample	Test 1	Test 2	Mean	Relative error
PEO-PDMS composite	331.69	333.7	332.70	0.3%
PDMS	319.15	290.10	304.63	4.77%

In summary, from the test results above, the mechanical properties of PDMS does not change much with the addition of the surfactant PDMS-b-PEO but the hydrophilicity is significantly improved. The hydrophilic PEO-PDMS promises the hydrogel solution to be easily cast and fast flow into the microchannels of the porous PEO-PDMS matrix.

2.5 Fabrication of Interconnected Porous PEO-PDMS by a Microsphere-Templating Process

In this research, an interconnected porous PEO-PDMS was fabricated by a microsphere templating process, which allows for the well-defined porous structured PEO-PDMS. White jojoba wax microspheres were obtained from Bramble Berry Inc. The properties of the wax microspheres are shown in Table 7.

Table 7: Properties of wax microspheres [54]

Sample	Average diameter (μm)	Melting temperature (˚C)	Density (g/cm^3)
Jojoba wax microspheres	260	67-75	0.86

The wax microspheres were sintered at 72˚C for 5 hours to form an interconnected wax template. Figure 34 shows a comparison of wax beads before sintering and after sintering observed under optical microscope from Zeiss® microscopy. It is noticeable that two neighboring wax beads were sintered together and formed an interconnected template. The Sylgard-184 base, curing agent and PDMS-b-PEO were mixed with a weight ratio of 100:10:1 and degassed in a vacuum desiccator for 1 hour. Then the mixture was slowly cast into the wax template and wait for one hour to allow the mixture to cast and penetrate into the wax template. After that, the sample was cured in oven at 40˚C for 72 hours. A relatively low curing temperature was chosen to avoid melting of wax beads. After PEO-PDMS was cured, the wax template was extracted by heating the sample above the melting temperature of the wax beads and mechanically squeezing out the wax template until the sample weight becomes constant. After that, the porous PEO-PDMS was immersed in an acetone bath at 50˚C with 500 rpm stirring for 48 hours to further remove residual wax on the surface of the sample. Figure 35 shows an image of a porous PEO-PDMS sample. Figure 36 shows a comparison of SEM images of a porous PEO-PDMS before the wax template removal and after the template removal. Figure 37 shows SEM images of the pores in a porous PEO-PDMS sample.

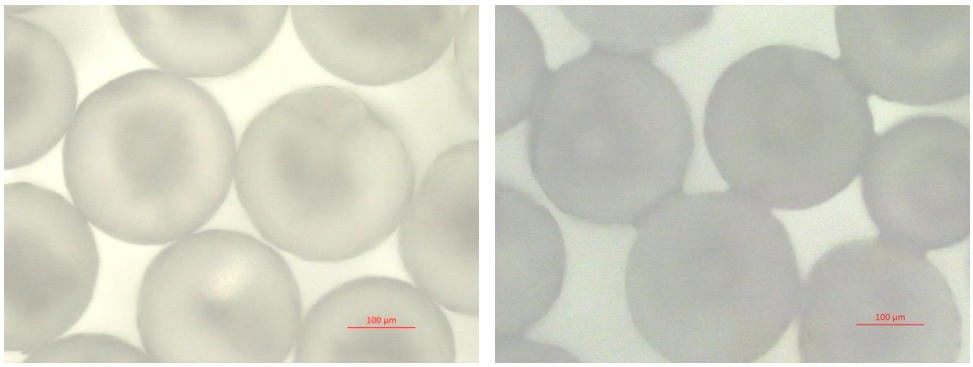

Figure 34: Wax beads before sintering (left) and after sintering (right)

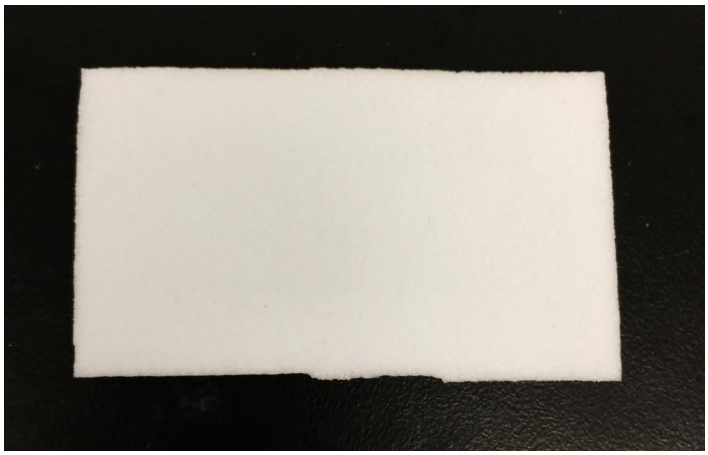

Figure 35: A porous PEO-PDMS sample

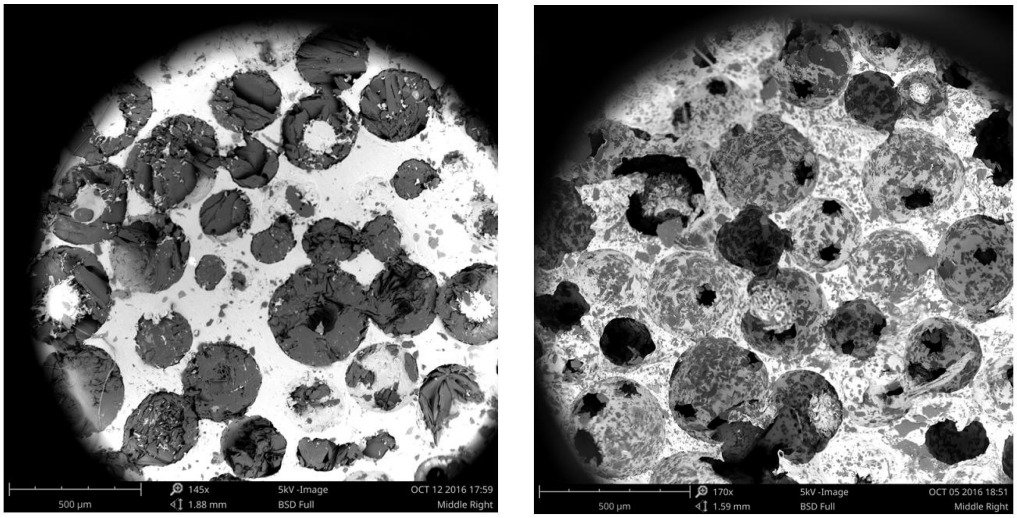

Figure 36: Porous PEO-PDMS before wax template removal (left) and after template removal (right)

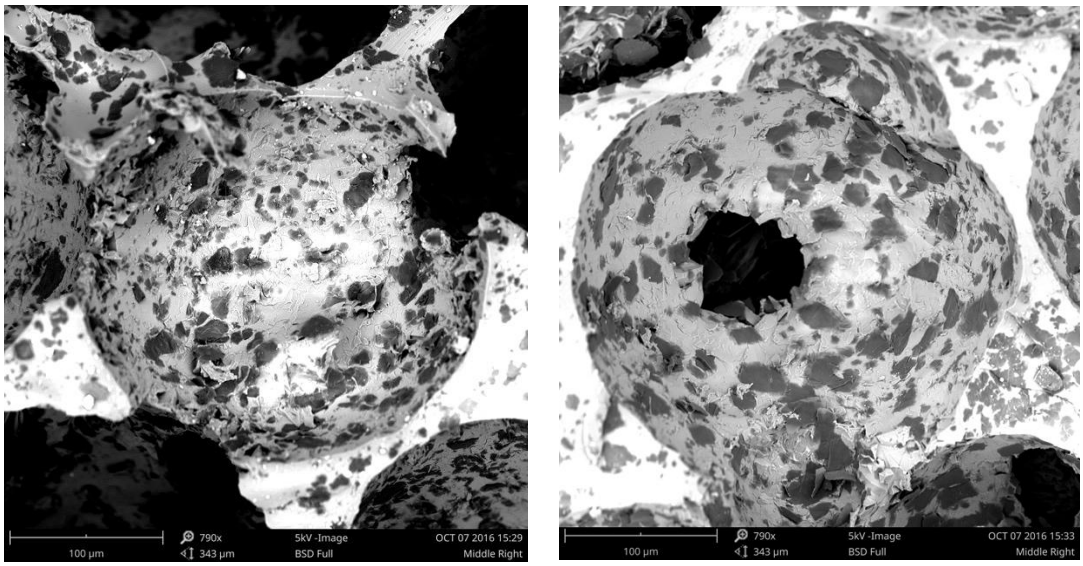

Figure 37: Pores in porous PEO-PDMS

2.6 Volume Fraction of Pores in Porous PEO-PDMS

The volume fraction of pores in a porous PEO-PDMS was determined by calculating the weight change of the sample before and after the wax template removal. Assuming the air volume in the sample is negligible, the volume fraction of pores can be calculated by:

$$\upsilon = \frac{\frac{w_1}{\rho_1}}{\frac{w_1}{\rho_1} + \frac{w_2}{\rho_2}} \tag{5}$$

where w_1 is the sample weight before wax template removal, w_2 is sample weight after template removal, ρ_1 is the density of wax beads, and ρ_2 is the density of PEO-PDMS. In this test, the density of wax beads is 0.86 g/cm^3 and the density of PEO-PDMS is 1.1 g/cm^3. Table 8 summaries the volume fraction test results of three porous PEO-PDMS samples.

The results are very consistent across the three samples, and the average volume fraction of pores is 53% in the PEO-PDMS sample.

Table 8: Volume fraction calculations of porous PEO-PDMS

Sample weight	#1	#2	#3
Before wax template removal	21.53g	28.44g	23.41g
After wax template removal	11.56g	15.09g	12.56g
Volume fraction of wax template	52.45%	53.09%	52.49%

2.7 Stress-strain Behavior of Interconnected Porous PEO-PDMS

The stress-strain behavior of a porous PEO-PDMS was characterized by a tensile test. A porous PEO-PDMS sample with a size of 7.90mm x 4.74mm x 3.40mm was clamped on DMA Q800, and a tensile stress was applied with a forcing rate of 2N/min until it reached 2N. Figure 38 shows the stress-strain response of a porous PEO-PDMS sample. Elastic modulus was calculated to be 249.1kPa by linear fitting the strain from 5% to 10%. Compared to the bulk PEO-PDMS, the modulus of porous PEO-PDMS is reduced by 82% due to the interconnected porous structure.

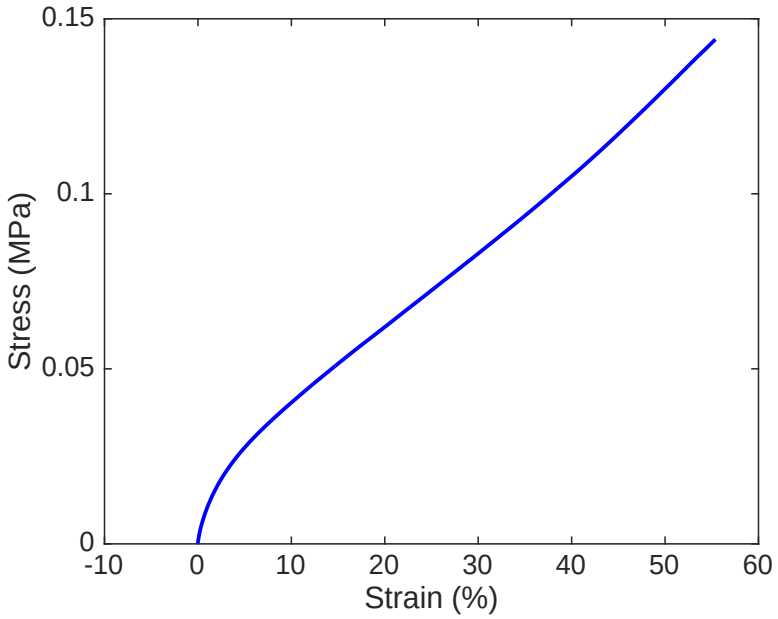

Figure 38: Stress-strain behavior of porous PEO-PDMS

Chapter 3

Fabrication and Characterization of Hydrogels

This chapter discusses the fabrication and characterization of two hydrogels, polyacrylamide hydrogel and PEG-HEA hydrogel. In this research, polyacrylamide hydrogel is selected as the interconnected hydrogel domains in the proposed elastomer-hydrogel composite to provide high water permeability and salt diffusivity. This chapter first discusses the fabrication procedures of polyacrylamide hydrogels, followed by the characterization of the hydrogel, swelling ratio test and compression test. In addition, this research explores the feasibility of using PEG-HEA hydrogel in the composite in which the fabrication and characterization tests are also discussed in this chapter.

3.1 Fabrication of Polyacrylamide Hydrogels

Recently, hydrogels have been widely used as a scaffold for drug delivery, tissue engineering, and biomedical applications [55]. Hydrogels are hydrophilic polymer networks that are physically entangled or chemically crosslinked with high water retention capacity [56]. Water molecules are either bonding to polar hydrophilic groups as ‘bond water’ or filling the space in the polymer chain network or pores as ‘free water’ [57]. Polyacrylamide hydrogel is a colorless, non-degradable, atoxic water gel that is widely used in drug treatment, ophthalmic operations, and water purification [58]. In this research, polyacrylamide hydrogel is filled in the pores of PEO-PDMS matrix to provide an interconnected path for molecules to diffuse through. This section discusses the fabrication of polyacrylamide hydrogels, and next section discusses the characterization of the

hydrogels including swelling ratio tests and compression tests.

In the fabrication process, a beaker filled with deionized (DI) water was first placed in the oven to saturate the oven chamber with a hydrated environment. This minimizes the water evaporation during the hydrogel curing process. Acrylamide monomer (AM, MW=71.08g/mol) from Sigma-Aldrich® was dissolved in DI water with a weight percent of 25%. Then the crosslinker N,N'-methylenebisacrylamide (MBAA, 0.06% the weight of AM), the initiator ammonium persulfate (AP, 0.17% the weight of AM), and the crosslinking accelerator N,N,N',N'-tetramethylenediamine (TEMED, 0.05% the weight of AM) were added and fully stirred for 2 minutes. The solution was then poured into a petri dish and degassed for 15 minutes. Finally, the hydrogel solution was cured in the oven at 50ºC for 5 hours. Figure 39 shows an as-prepared polyacrylamide hydrogel sample.

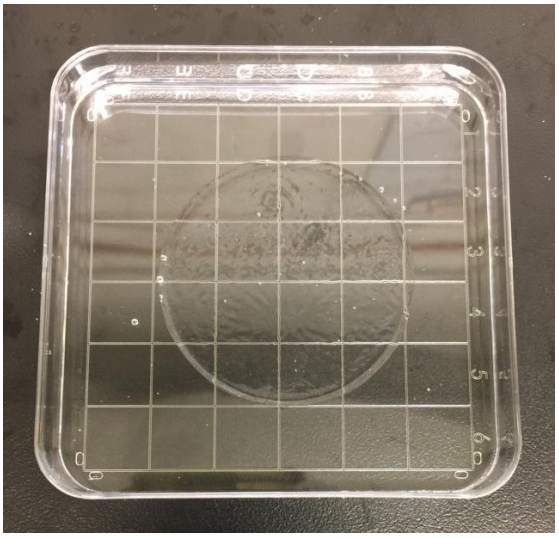

Figure 39: An as-prepared polyacrylamide sample

3.2 Characterization of Polyacrylamide Hydrogels

3.2.1 Swelling Ratio Test

A crosslinked hydrogel swells as water or solvent diffuses into the hydrogel network. The swelling properties describe the degree of swelling of a hydrogel network, which depends on crosslink density, solvent nature, and polymer-solvent interaction [56]. In this section, the volumetric swelling ratio of polyacrylamide hydrogel is tested and analyzed. The water induced volumetric swelling ratio Q of hydrogel can be calculated by:

$$Q = \frac{v_{swollen}}{v_{as-prepared}} \tag{6}$$

where $v_{swollen}$ is the volume of a swollen hydrogel and $v_{as-prepared}$ is the volume of an as-prepared hydrogel. In this test, a rectangular shaped as-prepared hydrogel sample with an initial volume of 0.9 ml was immersed in DI water in a cylinder, as shown in Figure 40. After 48 hours, the hydrogel was fully swollen and the sample volume was increased to 2.9 ml. Thus, the volumetric swelling ratio of polyacrylamide hydrogel is 3.2.

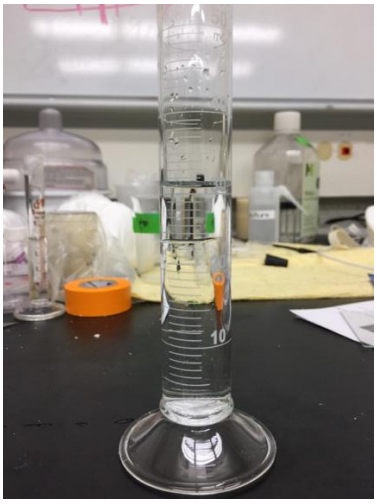

Figure 40: Volumetric swelling of polyacrylamide hydrogel

Water retention capacity of the hydrogel was also tested and analyzed. The water retention suggests the amount of water that can diffuse into and stored in the hydrogel network. An as-prepared hydrogel was placed in a desiccator with drierite for three days and the weight of the dried hydrogel sample was measured. Then the sample was immersed in DI water until the sample became swollen and the weight of the swollen sample was also measured. Figure 41 shows the three swelling conditions of a hydrogel sample, dried, as-prepared, and swollen condition. The weight of the hydrogel sample under different swelling conditions is summarized in Table 9. The weight ratio of swollen to as-prepared to dried hydrogel is 13.85:3.33:1.

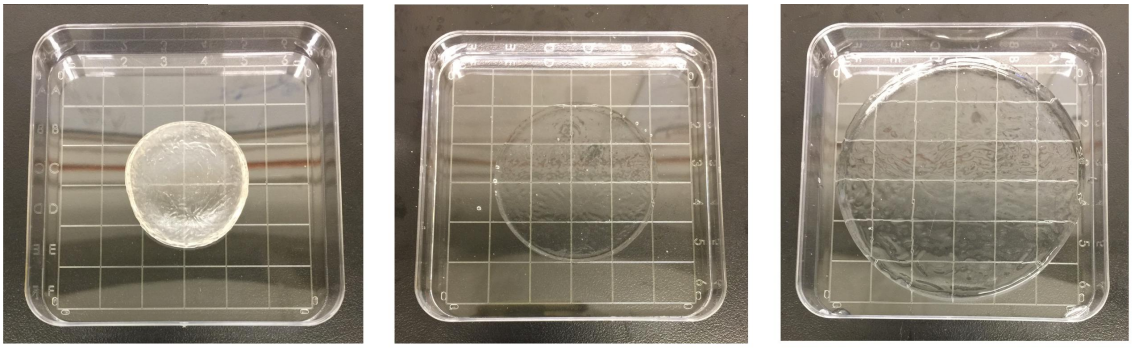

Figure 41: Different swelling conditions of a polyacrylamide hydrogel sample: dried (left), as-prepared (middle), swollen (right)

Table 9: The weight of polyacrylamide hydrogel under dried, as-prepared, and swollen condition

Swollen condition	Dried	As-prepared	Swollen
Weight (g)	2.17	7.23	30.09

3.2.2 Compression Test

Compression test is a common technique to determine the mechanical stiffness of a hydrogel. Traditional method such as tensile test is difficult to set up because hydrogels are slippery and compliant. The compression test involves placing the hydrogel sample under a compression plate and quickly compressing it to obtain the stress-strain response. Figure 42 shows the experimental setup for the compression tests. In this test, a rectangular shaped swollen hydrogel sample with a size of 17.2mm x 17.2mm x 8.2mm was glued to the bottom of a glass jar to avoid movement or instability of the sample during the loading process. Then DI water was added to the glass jar until the compression plate and the hydrogel were fully immersed in DI water. A preload of 0.1N was applied to the sample to ensure the sample surface was contacted with the loading plate and to stabilize the sample during the loading process. After that, a compressive loading rate of 10mm/min was applied to the sample until 60% strain was reached. A relatively high loading rate was used so that the water molecules do not have enough time to diffuse out of the deformed sample. The hydrogel is assumed to be incompressible and the compression response is equivalent to deformation of an elastic sample. Total of three compression tests were conducted. The true stress vs. strain response of the hydrogel sample is plotted in Figure 43, and the stiffness results are summarized in Table 10. The stiffness of the hydrogel was calculated by linear fitting the stress-strain data. The average elastic modulus of a swollen polyacrylamide hydrogel is 23kPa.

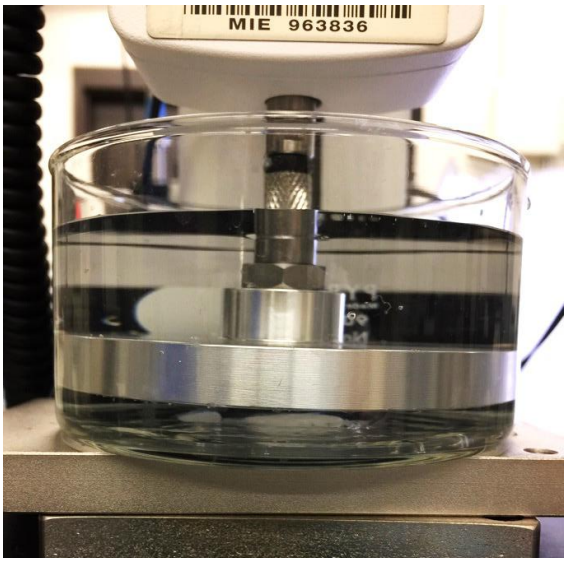

Figure 42: Experimental setup for compression tests of polyacrylamide hydrogels

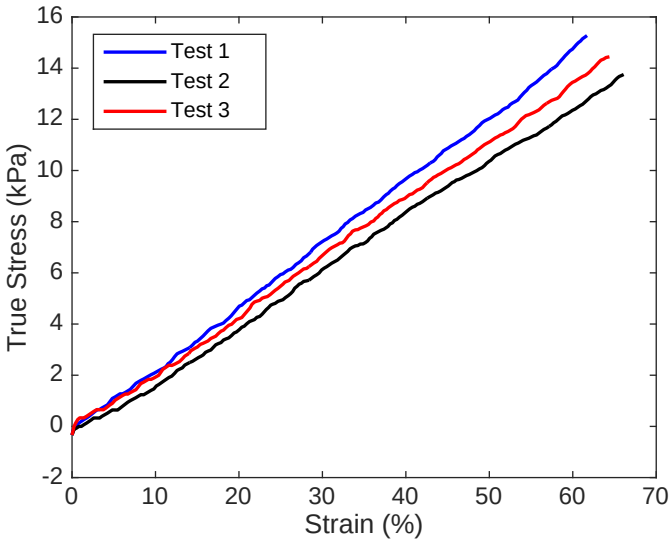

Figure 43: True stress vs. strain response of polyacrylamide hydrogel

Table 10: Elastic modulus test results of polyacrylamide hydrogel

Test	Test 1	Test 2	Test 3	Mean
Elastic modulus (kPa)	24.7	21.5	22.7	23

3.3 Fabrication of PEG-HEA Hydrogel

This section explores the feasibility of using another hydrogel, poly(ethylene glycol) (PEG)-based hydrogel, in the PDMS-hydrogel composite. PEG-based hydrogel has a high swelling ratio with potentials in fouling-resistant coating materials.

The hydrogel was synthesized by the crosslinker poly(ethylene glycol) diacrylate (PEGDA: MW=698, n=13), 2-hydroxyethyl acrylate (HEA: MW=116 g/mol, n=1), and the photoinitiator 1-hydroxycyclohexyl phenyl ketone (HPK). Prepolymerization mixture was first prepared by combining 60 mol% of PEGDA and 40 mol% of HEA with 1 wt% of photo-initiator. The crosslinker, monomer, and photoinitiator were then mixed in a glass jar and stirred with a magnetic stir bar for about one hour to completely dissolve the photoinitiator. The mixture was prepared in a UV-light filtered fume hood to minimize the light exposure to the solution. When the photoinitiator was fully dissolved, 60% wt% of DI water was added into the mixture and the solution was stirred for an additional hour. Then, the prepolymerization mixture was poured between two glass sheets with a layer of tape as spacers to control film thickness, as shown in Figure 44. In this test, the thickness of PEG hydrogel film is 330 μm. After that, the prepolymerization mixture was exposed to UV light for 120s for curing. Finally, the hydrogel film was rinsed and immersed in DI water for over 24 hours.

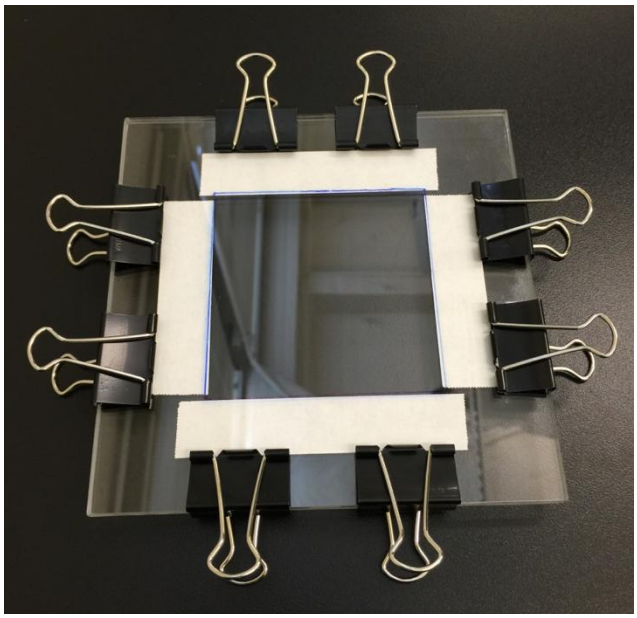

Figure 44: Apparatus for hydrogel thin film preparation

3.4 Characterization of PEG-HEA Hydrogel

3.4.1 Compression Test of PEG-HEA Hydrogel

The stretchability test of PEG based hydrogel was characterized by a uniaxial compression test because the sample is fragile and difficult to clamp. The aim of this test is to characterize the ultimate strain limit of the hydrogel when it reaches the failure point. A square shaped swollen PEG-HEA hydrogel sample (9mm×9mm) with a thickness of 3mm was first prepared. The sample was immersed in DI water to avoid water evaporation during the testing process. An increasing compressive load was applied to the sample using a Mark-10 load stand with a loading rate of 2mm/min. Because of the high loading rate, the poroelasticity of the sample is negligible and the sample is assumed to be incompressible. When the sample reaches its ultimate strain limit, the sample fractured into

pieces and a dramatic drop in stress was observed. Figure 45 shows a hydrogel sample before and after a compression test.

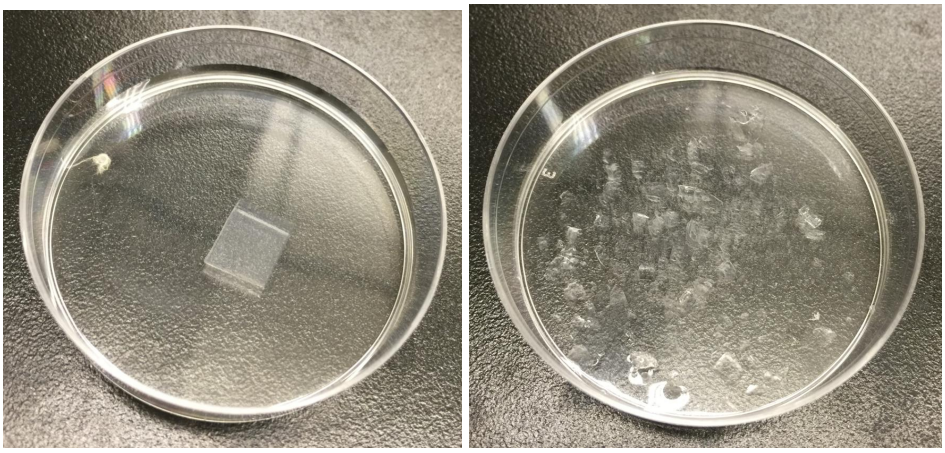

Figure 45: Hydrogel sample before and after a compression test

Total of three compression tests were conducted. Figure 46 shows the stress-strain behavior of PEG-HEA hydrogel. The stress-strain response behaves non-linearly in the initial loading stage because water was squeezed out from the bottom of the sample. It was assumed that the loading plate was fully contacted with the sample surface when the slope of stress versus strain curve became relatively constant. Since the hydrogel sample was deformable so true stress was used in this analysis assuming that the material is incompressible. If we take the full contact point as the starting point, the hydrogel sample fractured at a compressive stress of 0.5MPa and the corresponding strain is 0.153. The test results show low stretchability of PEG-HEA hydrogel, and the material is very fragile even at a low compressive load. Polyacrylamide hydrogel exhibits a relatively higher stretchability than PEG-HEA hydrogel in terms of mechanical robustness.

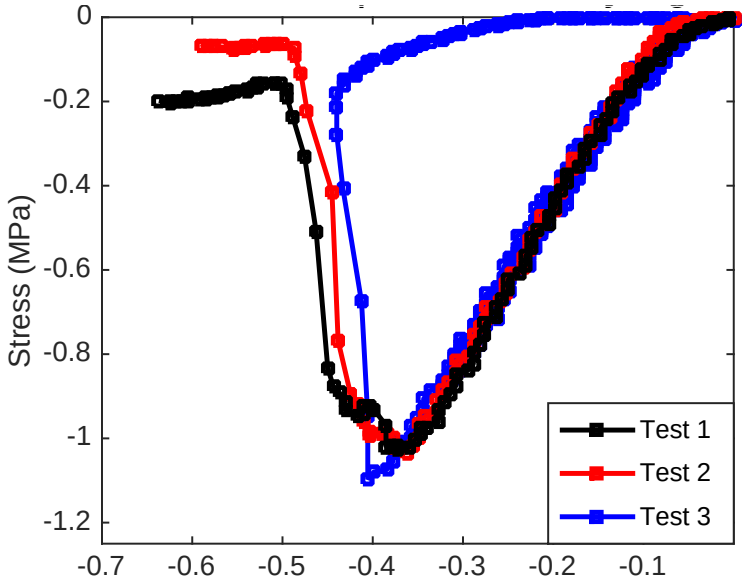

Figure 46: Stress-strain behavior of a PEG-HEA hydrogel under a compressive load

3.4.2 Water Permeability Test of PEG-HEA Hydrogel

This section discusses the characterization of water permeability of PEG-HEA hydrogel by a pressure-driven diffusion process. The permeability test was conducted using a 50 mL Amicon 8050 filtration cell from Millipore Corp, as shown in Figure 47. The cell is consisted of four parts: a top cap, body, membrane support, and a bottom fitting. The hydrogel sample was placed into the filtration cell, and the O-ring completely covered and constrained the membrane edges. Figure 48 shows a schematic of the testing system. Ultrapure water was prepared in the filtration cell, and the filtration cell was pressurized by inert nitrogen gas. The applied pressure was regulated using a pressure regulator from Airgas Inc. based on the pressure reading of a pressure transducer from OTC Inc. The applied pressure forced water to permeate through the hydrogel membrane. Water permeated through the membrane flowed out from the permeate tube attached at the bottom

of the filtration cell and collected in a flask. Figure 49 shows the assembled experimental apparatus.

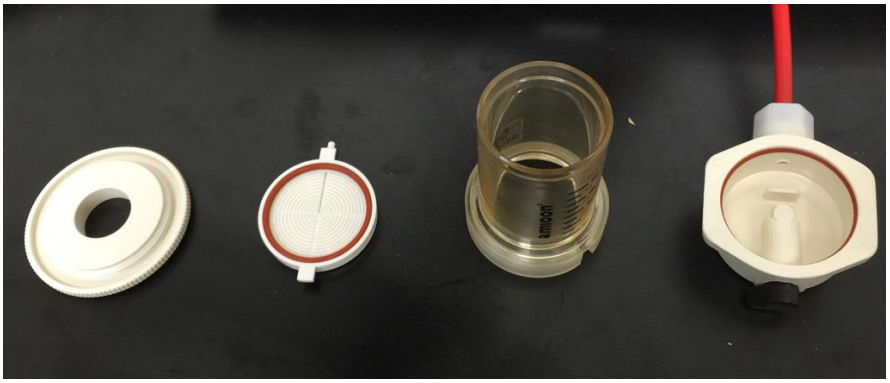

Figure 47: Filtration cell for permeability test

Considering the low water flux permeated through the membrane, in this test, water flux was measured by counting the water droplets coming out of the tube that attached to the bottom of the filtration cell. Water evaporation effect has a low impact on this method because a water droplet has a small surface area and short air exposure time. The water droplets were recorded by using a CCD camera, and a picture was taken every one minute. Assuming the size of each droplet is the same, the water flux can be calculated by $\Delta m/\Delta t$. A small amount of water was added to the flask before the test to saturate the humidity in the flask. The weight of each water droplet was calibrated as 0.049 ± 0.0005g.

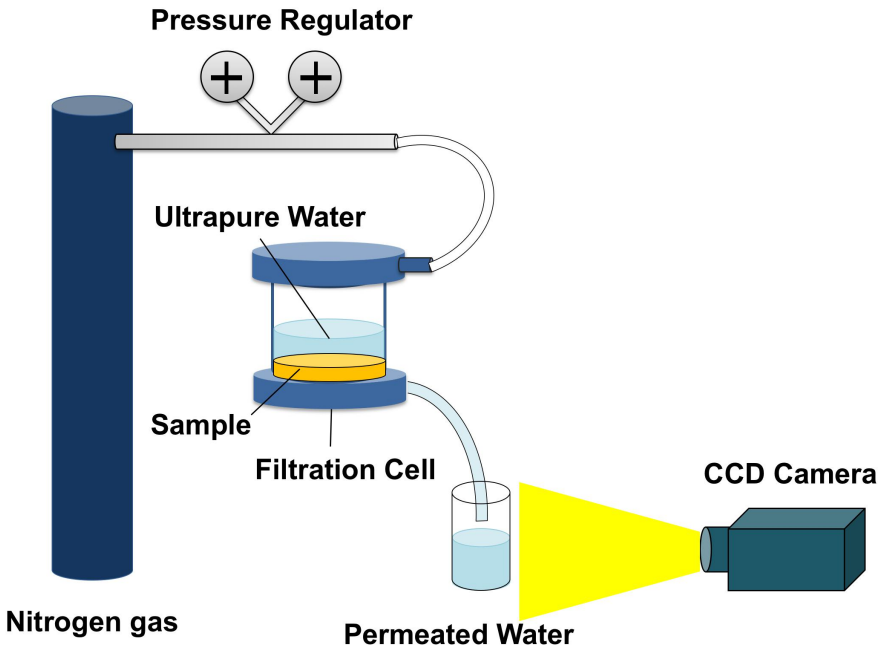

Figure 48: Schematic of permeability testing system

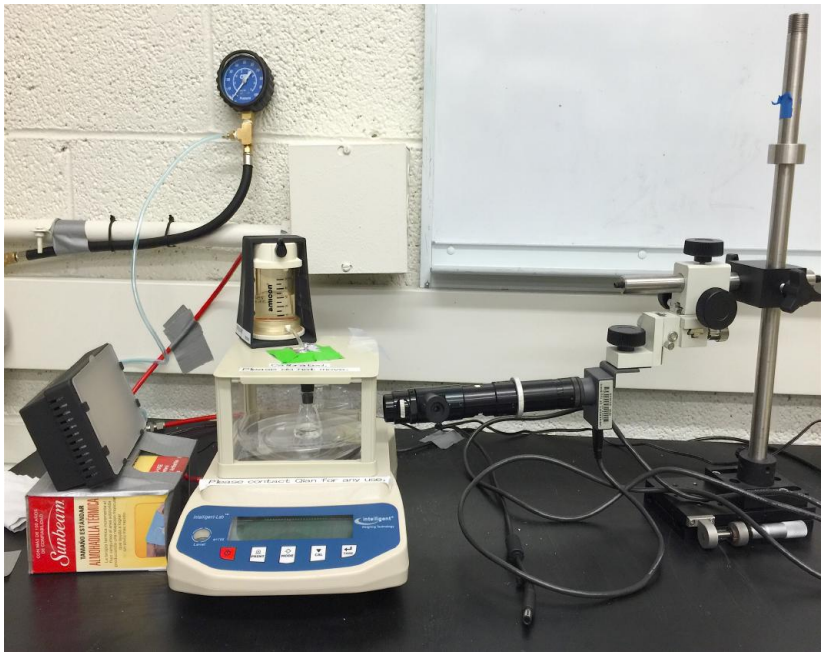

Figure 49: Assembled permeability testing system

Figure 50 shows the formation of a water droplet over time where the image framing rate is one image per minute. The water permeability can be calculated using the following equation:

$$P = \frac{\Delta V l}{A \Delta p t} \tag{7}$$

where P is water permeability, ΔV is the volume of water permeated through the membrane, l is the film thickness, A is contact surface area of the membrane, Δp is the differential pressure, and t is the testing time. The thickness of the sample is 315μm, the contact area of the membrane is 12.57cm^2, and the applied gage pressure is 156.86kPa. The time between two successive water droplets is 27 minutes. Therefore, the water permeability is calculated to be 18.26 ($\frac{L*um}{m^2*hr*bar}$).

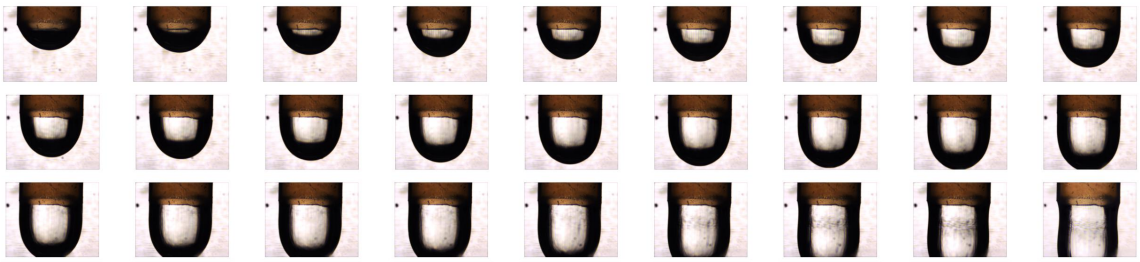

Figure 50: Water droplet formation process in water permeability test

In summary, PEG-HEA hydrogel has a high water permeability but a low stretchability. PEG-HEA hydrogel can be a potential material to be integrated into an elastomer porous structure to provide the functionality. In this research, polyacrylamide was selected as the hydrogel domains in the PDMS-hydrogel composite because it is easy to make and less fragile than PEG-HEA hydrogels.

Chapter 4

Design, Fabrication, and Characterization of PDMS-Hydrogel Composite

This chapter discusses the fabrication process of co-continuous PDMS-hydrogel composite. The composite consists of an interconnected porous PEO-PDMS elastomer matrix with interconnected polyacrylamide hydrogel domains. The PDMS-hydrogel composite combines the stretchability of PEO-PDMS and the high water permeability of hydrogels. In addition, the well-defined PEO-PDMS porous structure provides the encapsulation of hydrogels, which allows for high water retention capacity and low water evaporation rate. The characterization of the PDMS-hydrogel is also presented in this chapter, including swelling ratio test, DMA tensile test, compression test, and salt diffusivity test, which aid in understanding the material properties of the composite.

4.1 Fabrication of PDMS-Hydrogel Composite

In the fabrication process, a porous PEO-PDMS sample and polyacrylamide solutions were prepared. Then the porous PEO-PDMS was placed in a petri dish and hydrogel solution was slowly poured into the petri dish until the PEO-PDMS was fully immersed. After that, the sample was compressed to remove air trapped in the porous PEO-PDMS and to allow hydrogel solutions to flow into the pores. The sample was then moved to a vacuum desiccator and degassed for 15 minutes to further remove the air bubbles. This step needs to be handled very quickly in case the hydrogel starts to cure and becomes viscous. Until no air bubble was observed on the sample surface, degassing was terminated and the

sample was moved to oven for curing at 50ºC for 5 hours. Figure 51 shows a co-continuous PDMS-hydrogel composite. The filaments in the cutting cross section are the stretched interconnected hydrogel domains. Figure 52 shows the stretching process of a cutting cross section of a PDMS-hydrogel composite.

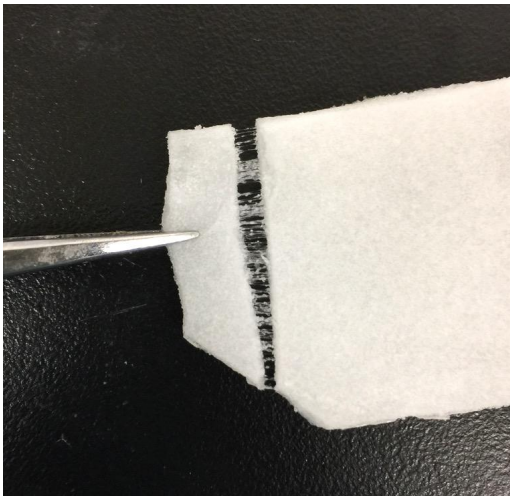

Figure 51: A PDMS-hydrogel composite with a cutting cross section

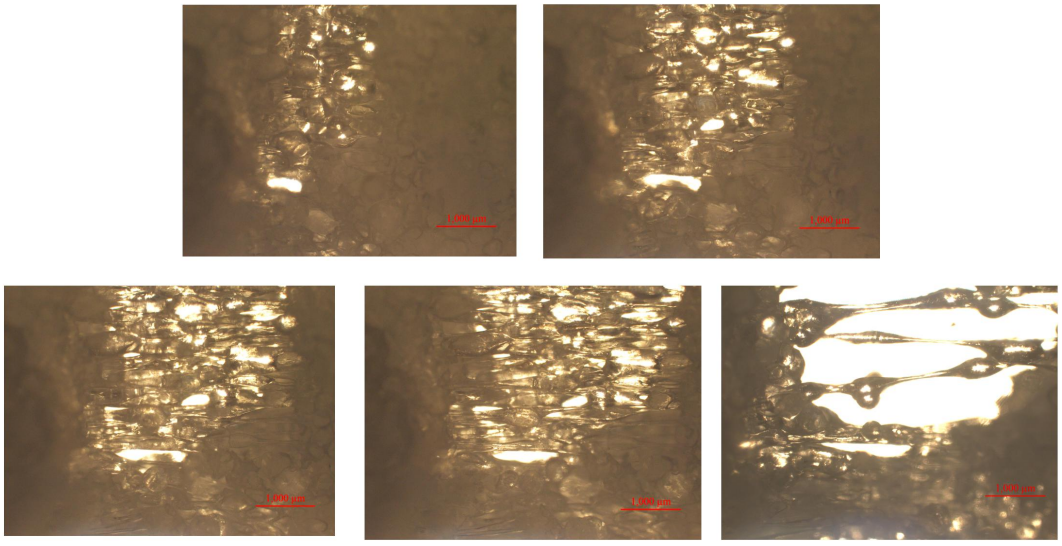

Figure 52: The stretching process of a cutting cross section of a PDMS-hydrogel composite

The internal microstructure of a cross section of a swollen PDMS-hydrogel composite was observed in SEM. A swollen PDMS-hydrogel sample was placed on a foam and frozen by liquid nitrogen. When the sample was frozen by the liquid nitrogen, a small slice was cut from the sample with a neat and clean cross section. After that, the sample slice was quickly observed under SEM to minimize water evaporation. Figure 53 shows SEM images of a cross section of a swollen PDMS-hydrogel composite. It can be seen that the hydrogels are filled in the porous PEO-PDMS matrix with a co-continuous structure. The swelling of the hydrogels is constrained by the PEO-PDMS matrix due to its relatively higher stiffness. Figure 54 shows SEM images of a cross section of a PDMS-hydrogel composite after being left at room temperature (25ºC) for three hours. It can be seen from the figure that the hydrogel microspheres shrink and there is a gap between the hydrogel and the PEO-PDMS matrix. This is due to the time-dependent water evaporation in the hydrogels.

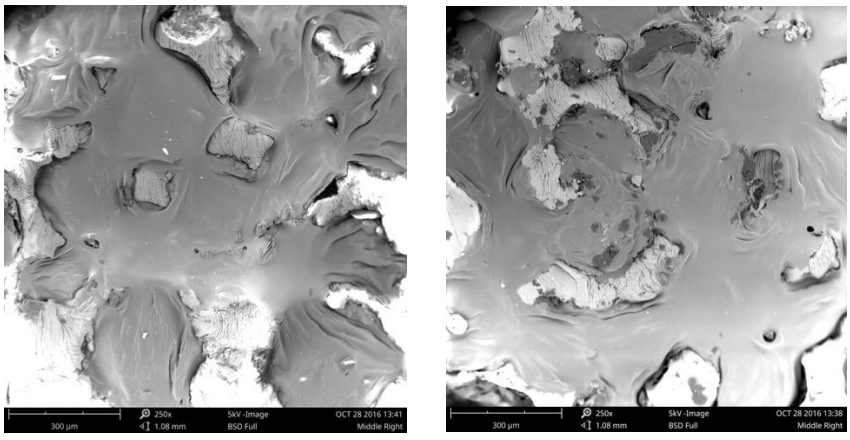

Figure 53: Cross section of a swollen PDMS-hydrogel composite

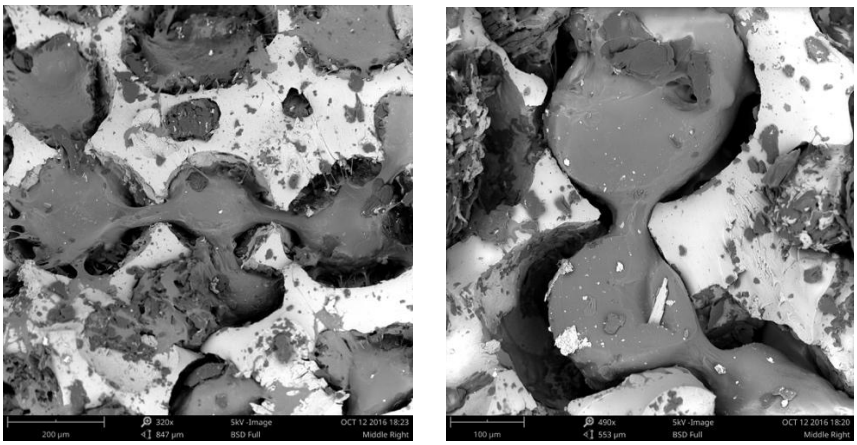

Figure 54: Cross section of a swollen PDMS-hydrogel composite after being left at room temperature for three hours

4.2 Simulation of PDMS-Hydrogel Composite under Mechanical Stretching by Finite Element Analysis

In a PDMS-hydrogel composite, the strain field of the hydrogel domain under mechanical stretching is analyzed by finite element analysis in Abaqus. Strain field at the center of hydrogel domains is compared to the stretch of the composite. This analysis aids in understanding the relationship between the applied stretch to the bulk composite material and the strain in the hydrogel domains. In this analysis, the composite is assumed to be a thin film with a symmetric configuration about x, y, z planes. So only one eighth of the composite unit was modeled to reduce the computation effort, as shown in Figure 55. The CAD model of the one eighth composite unit was created in Solidworks then imported into Abaqus for finite element analysis.

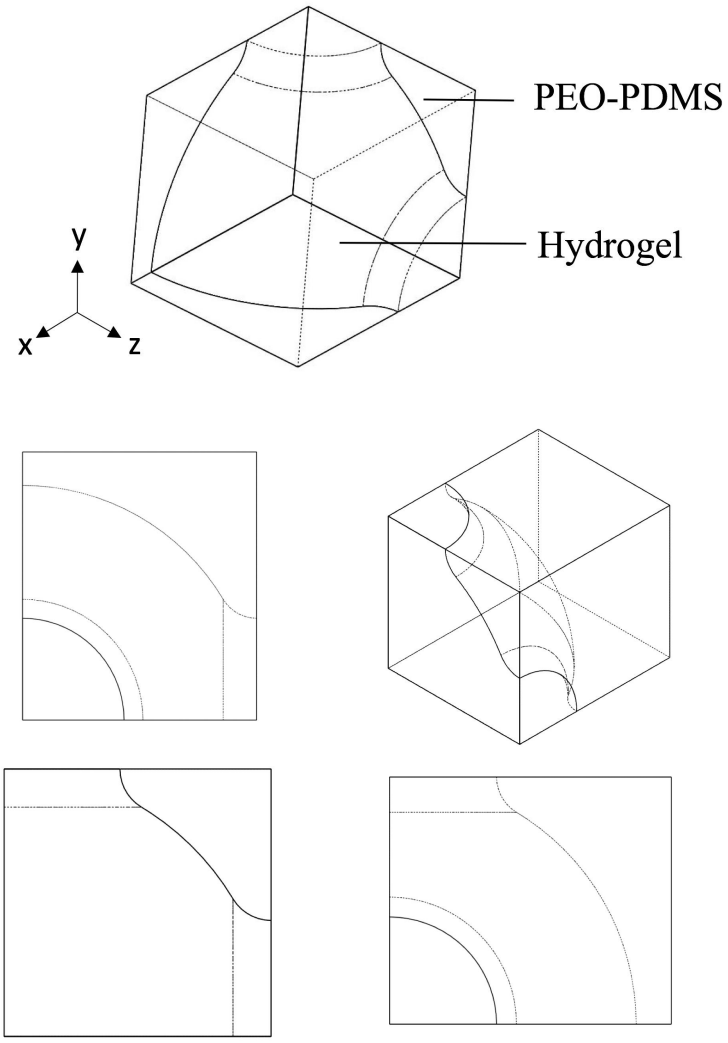

Figure 55: PDMS-hydrogel model in finite element analysis

In the analysis, the 3D homogeneous solid element type was used to model both PEO-PDMS and the hydrogel. The material property of each material was defined by the experimental characterization results where the elastic modulus of PEO-PDMS is 1.4 MPa and polyacrylamide hydrogel is 23 kPa. Assuming PEO-PDMS and hydrogel are incompressible, the Poisson's ratio of both materials is 0.5. Both materials were assumed to be hyperelastic and modeled using the Neo-Hookean model. Another assumption in this simulation is that PEO-PDMS and hydrogel are tie together. To increase the accuracy, the

composite model was meshed with quadratic tetrahedron elements. Three loading conditions were studied, stretching in x-axis and z-axis, and biaxial stretching in both x- and z-axis. Strain field at the center of hydrogel was extracted and analyzed. The simulation results of strain vs. stretch are shown in Figure 56. The simulation results show that as the bulk composite is stretched to 100% in x/z direction, the strain at the center of hydrogel is lower than 1. The strain loss is mainly caused by the compliance of elastomer matrix and hydrogel domains.

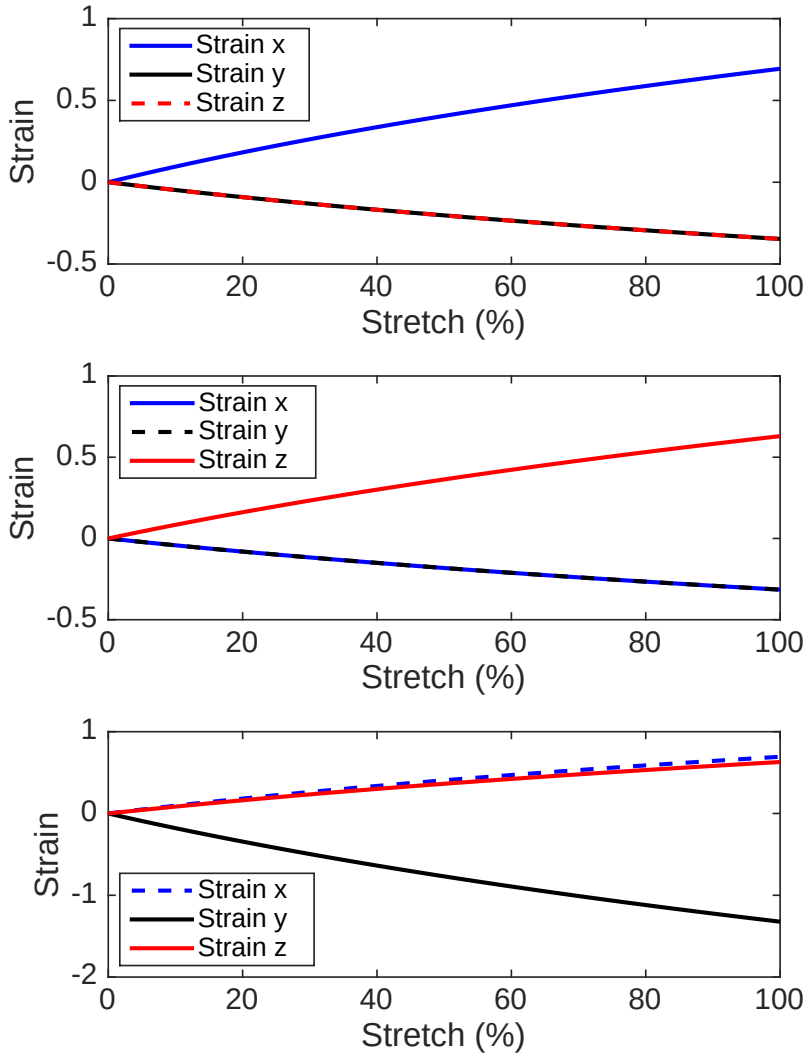

Figure 56: FEA results: strain vs. stretch in the center of hydrogel microsphere in PDMS-hydrogel composite

4.3 Characterization of PDMS-Hydrogel Composite

4.3.1 Swelling Ratio Test

In the PDMS-hydrogel composite, the PEO-PDMS matrix provides a swelling controlled porous structure that constrains the swelling of hydrogel domains. There is an opposite elasticity force from PEO-PDMS matrix that prevents the expansion of the hydrogel network. At equilibrium, the osmotic forces are balanced with the elasticity force. In this section, a volumetric swelling ratio test was conducted to analyze the expansion of hydrogel with the constrained porous structure. A rectangular shaped as-prepared sample with an initial volume of $1cm^3$ was immersed in DI water for over 48 hours. The sample volume was measured by placing the composite sample in a cylinder and measuring the water volume change. The volume of the swollen composite sample is 1.4 cm^3 so the swelling ratio is 1.4. Note that the swelling ratio (SR) of PDMS-hydrogel composite lies in between PEO-PDMS (SR=1) and polyacrylamide hydrogel (SR=3.2). Figure 57 shows a swollen PDMS-hydrogel composite. It can be seen that there are some hydrogels on the sample surface. Even though the PEO-PDMS constrains the swelling of the internal hydrogels, hydrogels on the composite surface can swell and free expand.

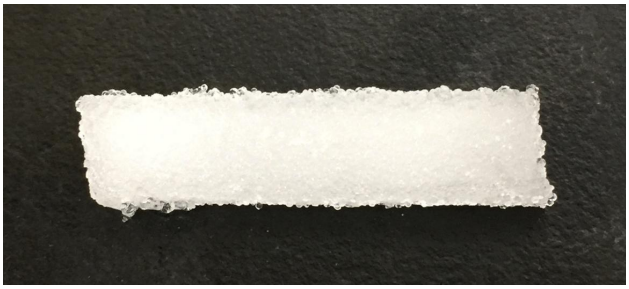

Figure 57: A swollen PDMS-hydrogel composite

4.3.2 DMA Tensile Test

The stress-strain behavior of a swollen PDMS-hydrogel composite was characterized using DMA Q800. Figure 58 shows the experimental setup of the tensile test. A rectangular shaped sample with a size of 6mm x 6.5mm x 3.4mm was tested. A preload of 0.001N was applied to the sample, and an increasing tensile load was applied to 2N with a loading rate of 2N/min. Figure 59 shows the stress-strain behavior of a swollen PDMS-hydrogel sample. The elastic modulus was calculated to be 142.4kPa by linear fitting the stress-strain curve portion of strain from 5% to 10%. Compared to the porous PEO-PDMS, the modulus of PDMS-hydrogel is slightly lower. A possible reason for the decreased modulus is the expansion of porous structure due to the swelling of hydrogel. So the volume fraction of PEO-PDMS in a PDMS-hydrogel composite is lower than porous PEO-PDMS.

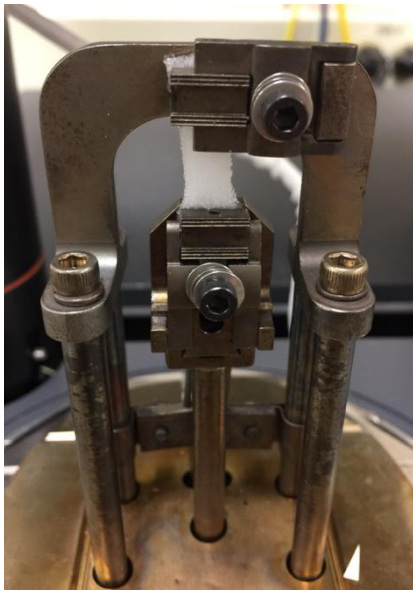

Figure 58: DMA tensile test of a PDMS-hydrogel composite

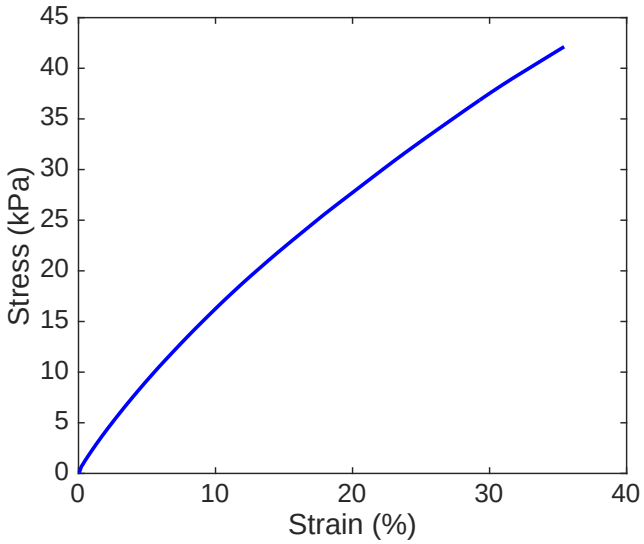

Figure 59: Stress-strain behavior of a swollen PDMS-hydrogel

4.3.3 Compression Test

In this section, a compression test of PDMS-hydrogel was conducted to further validate the elastic modulus characterized by DMA tensile test. A swollen PDMS-hydrogel composite with a size of 21.33mm x 22.27mm x 5.97mm was glued to the bottom of a glass jar, and sufficient water was added to the glass jar such that the sample and the loading plate were fully immersed in water. Figure 60 shows the experimental setup for the compression test. A preload of 0.1N was applied to the sample surface, and sequentially a compressive load was applied to the sample with a loading rate of 2mm/min using Mark-10 load stand. Figure 61 shows the true stress-strain behavior of the PDMS-hydrogel composite. The elastic modulus of the composite was estimated to be 136.1kPa by linear fitting the stress-strain curve section for 5%-10% strain. The nonlinearity at initial loading condition is due to water being squeezed out from the bottom of the sample. The modulus measured by the compression test is very close to the modulus tested from DMA tensile

test, with a relative difference of 4.4%.

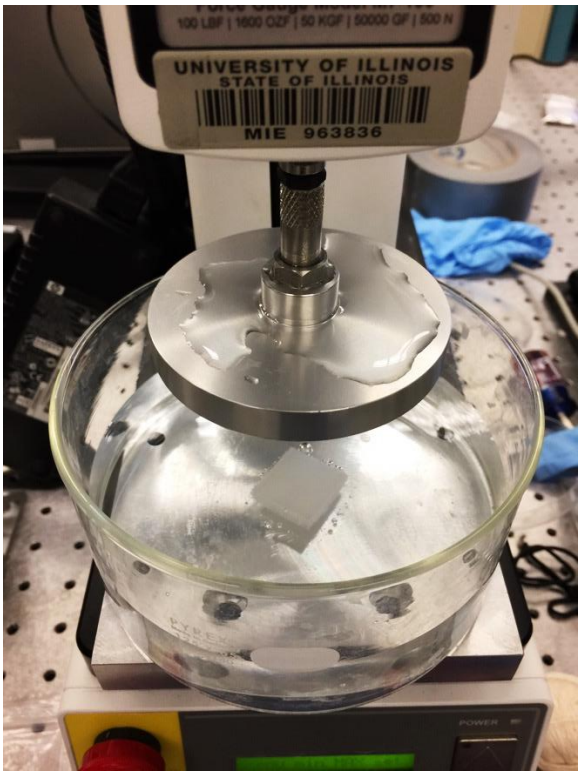

Figure 60: Experimental setup for compression test of PDMS-hydrogel composite

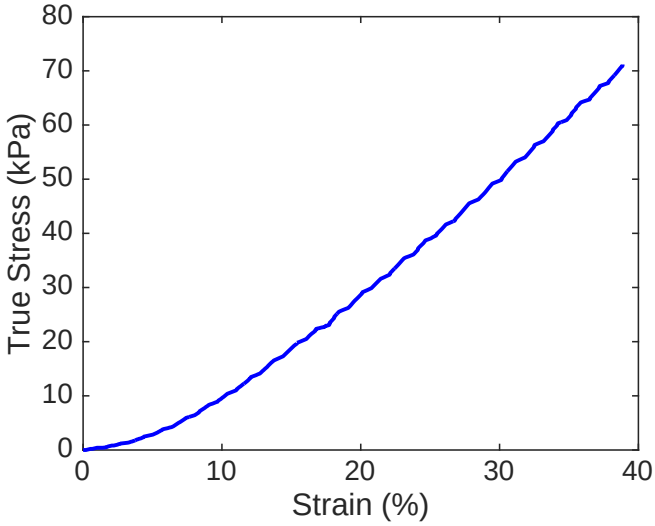

Figure 61: True stress vs. strain behavior of a PDMS-hydrogel composite

4.3.4 Salt Diffusivity Test

Salt transport property is important in drug delivery and tissue engineering. In this research, salt transport test in PDMS-hydrogel was performed using kinetic desorption experiments [59]. Two samples were prepared and tested, a PDMS-hydrogel film with a thickness of 2mm and a polyacrylamide hydrogel film with a thickness of 3.8mm. Both samples were immersed in 1M sodium chloride solutions for 48 hours. Then the samples were removed and quickly patted dry. After that, the sample was placed in a beaker with 100ml DI water. The beaker was sealed with Parafilm to minimum the water evaporation and reduce solution conductivity change due to the absorption of CO_2 in water. The experimental setup is shown in Figure 62. The solution was stirred at 500rpm to give a uniform salt concentration in the solution. Solution conductivity was measured using a conductivity meter PCE-PHD 1 from PCE Instruments. The sampling rate was 0.5Hz. The test was terminated as the conductivity of the solution became constant. That is, the sample and the salt solution reached an equilibrium. The test results are shown in Figure 63.

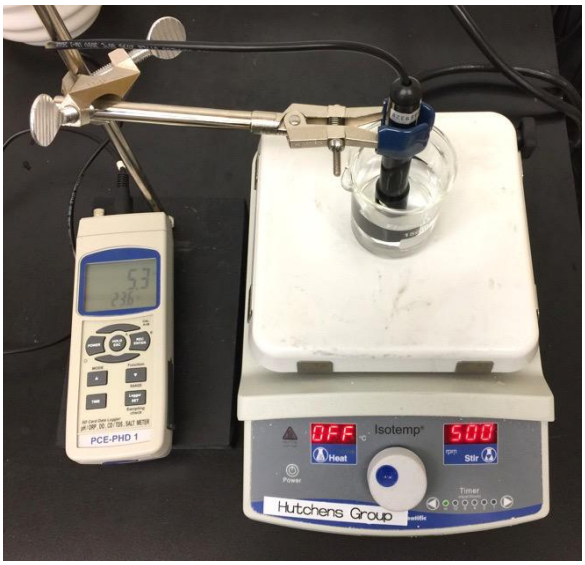

Figure 62: Experimental setup for kinetic desorption salt diffusivity test

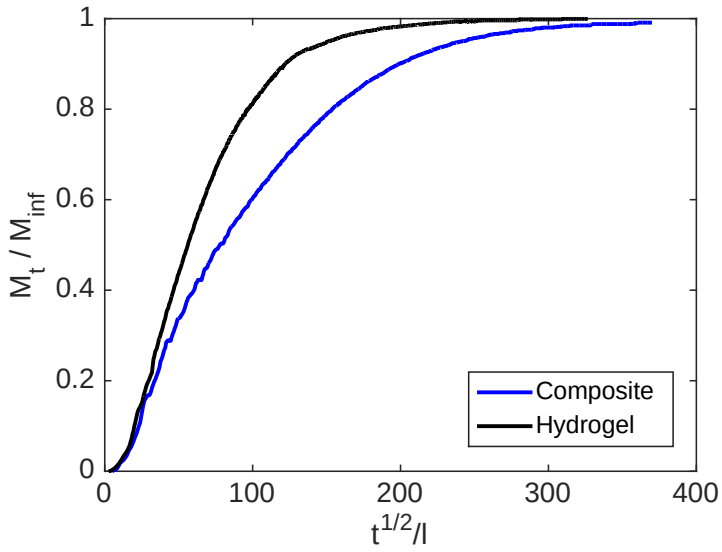

Figure 63: Kinetic desorption test results of PDMS-hydrogel composite and hydrogel

The salt diffusion coefficient *Ds* was calculated based on Fickian analysis of solution desorption from a planar film [60, 61]:

$$Ds = \frac{\pi l^2}{16}\left[\frac{d(M_t/M_\infty)}{d(t^{1/2})}\right]^2 \qquad [8]$$

where *l* is the sample thickness, $\frac{d(M_t/M_\infty)}{d(t^{1/2})}$ is the slope of the linear section of M_t/M_∞ versus $t^{1/2}$ plot, M_t is the instantaneous salt concentration of the solution, M_∞ is the equilibrium salt concentration of the solution, and *t* is time. A calibration curve of solution conductivity vs. salt concentration was characterized, as shown in Figure 64. The calibration curve shows a linear relationship of conductivity to salt concentration in the solution. So the ratio of M_t/M_∞ can be approximated as C_t/C_∞ where *C* is the conductivity of the solution. The salt diffusivity coefficient Ds was obtained by fitting the linear region of the curve that M_t/M_∞ between 0.1 and 0.6. The NaCl diffusion coefficient of PDMS-hydrogel composite is 5.62×10^{-6} cm^2/s and polyacrylamide hydrogel is 1.67×10^{-5} cm^2/s.

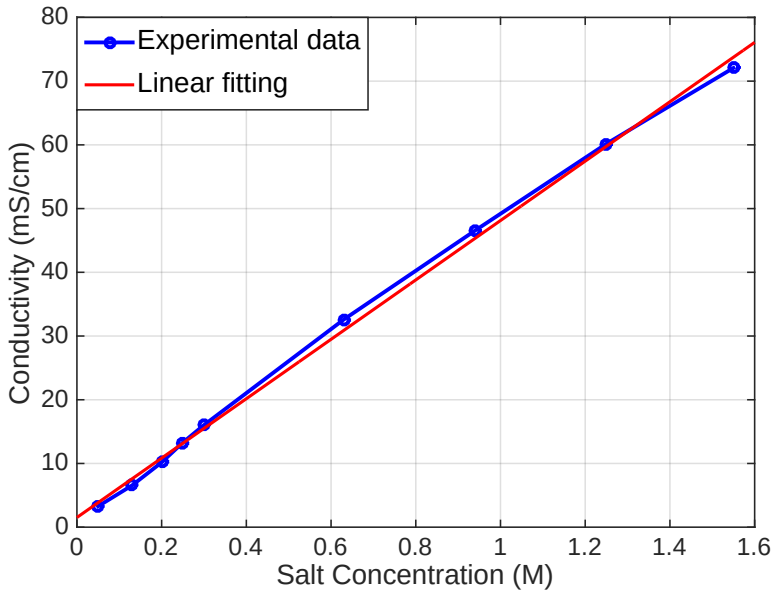

Figure 64: Conductivity calibration curve of solution conductivity vs. salt concentration

Chapter 5

Summary

In this research, an elastomer-hydrogel composite is designed, fabricated, and characterized. The composite consists of a porous interconnected hydrophilic PEO-PDMS matrix filled with cocontinuous polyacrylamide hydrogel domains, which combines the high elasticity of PEO-PDMS and the high water permeability of hydrogels. The encapsulation of hydrogel in PEO-PDMS matrix can also maintain high water retention of hydrogels. The aim of the material is to be used as a mechanically tunable sieve for drug delivery and tissue engineering. The hydrophilicity of PDMS is improved by the addition of a block copolymer poly(dimethylsiloxane-ethylene oxide polymeric) (PDMS-b-PEO). The stiffness, contact angle, and fracture energy of the hydrophilic PEO-PDMS were experimentally characterized and compared to the behavior of PDMS. The interconnected porous structure of PEO-PDMS was fabricated by a microsphere wax templating process, which gives a stable and well-defined porous structure. Polyacrylamide hydrogels were cast into the porous PEO-PDMS to form interconnected hydrogel domains. The PDMS-hydrogel composite was characterized by swelling tests, DMA tensile tests, and salt diffusivity tests to offer insights into the behavior of cocontinuous hydrogels in PEO-PDMS matrix. This research has provided an experimental guideline for the design of cocontinuous polymer blends with two immiscible materials for material properties enhancements.

Future work may include the improvement of the compatibility of the elastomer matrix with the hydrogel domains to promise controlled volume change in the porous

structure under mechanical stretching. Swelling tests with various crosslinking ratio of PDMS and various polymer fractions of hydrogels can aid in investigating the mechanism of PDMS and hydrogel interaction, the interplay of matrix material elasticity and swelling expansion of hydrogels. In addition, different pore sized matrices can be obtained by microsphere templates formed by different sized wax beads. So the effect of various volume fractions of hydrogels can be studied via different pore sized matrices to tune the material properties of the composite.

References

[1] H. Pernot, M. Baumert, F. Court, and L. Leibler. Design and properties of co-continuous nanostructured polymers by reactive blending. *Nature Materials* (2002).

[2] M. Trifkovic, A. T. Hedegaard, M. Sheikhzadeh, S. Huang, and C. W. Macosko. Stabilization of PE/PEO cocontinuous blends by interfacial nanoclays. *Macromolecules* (2005).

[3] Robeson, L. M. *Polymer Blends: A Comprehensive Review*. ISBN-13: 978-1-56990-408-4 (2007).

[4] Rajagopalan, V. N. Generation of multicomponent polymer blend microparticles using droplet evaporation technique and modeling evaporation of binary droplet containing non-volatile solute. Ph. D. Dissertation, University of Kentucky (2014).

[5] Henry, M. F. Solid-state compatibilization of immiscible polymer blends: cryogenic milling and solid-state shear pulverization. Master's Thesis, Bucknell University (2010).

[6] Young, N. P. Thermodynamics and phase behavior of miscible polymer blends in the presence of supercritical carbon dioxide. Ph. D. Dissertation, University of California, Berkeley (2014).

[7] Paul, D. R., Bucknall, C. B., Eds. *Polymer Blends;* Wiley: New York (1999).

[8] Lopez-Barron, C. R., Macosko, C. W., Characterizing Interface Shape Evolution in Immiscible Polymer Blends via 3D Image Analysis, *Langmuir*, 25(16), 9392-9404 (2009).

[9] Li, J. M., Ma, P. L., Favis, B. D., The Role of the Blend Interface Type on Morphology in Cocontinuous Polymer Blends, *Macromolecules*, 35, 2005-2016 (2002).

[10] Yuan, Z. H., Favis, B. D., Influence of the Efficacy of Interfacial Modification on the Coarsening of Cocontinuous PS/HDPE Blends During Quiescent Annealing, *J. Polym. Sci. Part B: Polym Phys*, 44, 711-721 (2006).

[11] Utracki L. A. & Wilkie C. A. *Polymer Blends Handbook*. ISBN: 978-94-007-6063-9 (2003).

[12] Macosko, C. W.; Guegan, P.; Khandpur, A. K.; Nakayama, A.; Marechal, P.; Inoue, T. *Macromolecules*, *29*, 5590-5598 (1996).

[13] C. Harrats, N. Makhilef, Predictions, generation and practical applications, in Micro- and Nanostructured Multiphase Polymer Blend Systems, ed. by C. Harrats, S. Thomas, G. Groeninckx (Taylor and Francis, Boca Raton, 2006b).

[14] Pyun, A., Bell, J. R., Won, K. H., Weon, B. M., Seol, S. K., Je, J. H., Macosko, C. W., Synchrotron X-ray Microtomography for 3D Imaging of Polymer Blends, *Macromolecules*, 40, 2029-2035 (2007).

[15] Zhang, W. Controllable growth of porous structures from co-continuous polymer blend. Ph. D. Thesis, Georgia Institute of Technology (2011).

[16] Hedegaard, A. T. Cocontinuous polymer blends: controlling morphology via interfacial modification and rheology. Ph. D. Dissertation, University of Minnesota (2014).

[17] Ramachandran, R., Dinunzi, S. A. US Patent #5589545 A (1994).

[18] Lu, Q., Meltzer, D. A., Eckstein, Y. US Patent #2011/0092648 A1 (2010).

[19] RTP Company Permastat® Compounds Providing Permanent Antistatic Protection - Conductive and Antistatic Plastic Compounds.

[20] Galloway, J. A., Koester, K. J., Paasch, B. J., Macosko, C. W., Effect of sample size on solvent extraction for detecting cocontinuity in polymer blends, *Polymer*, 45, 423-428 (2004).

[21] Riscanu, D., Favis, B. D., Feng, C., Matsuura, T., Thin-film membranes derived from co- continuous polymer blends: preparation and performance, *Polymer*, 45, 5597-5609 (2004).

[22] Lopez-Barron, C., Macosko, C. W. Characterizing Interface Shape Evolution in Immiscible Polymer Blends via 3D Image Analysis, *Langmuir*, 25, 9392-9404 (2004).

[23] Trifkovic, M., Hedegaard, A., Huston, K. Sheikhzadeh, M., Macosko, C. W., Porous Films via PE/PEO Cocontinuous Blends, *Macromolecules*, 45, 6036-6044 (2012).

[24] Sarazin, P., Roy, X., Favis, B. D., Controlled preparation and properties of porous poly(l-lactide) obtained from a co-continuous blend of two biodegradable polymers, *Biomaterials*, 25, 5965-5978 (2004).

[25] Washburn, N. R., Simon, C. G., Tona, A., Elgendy, H. M., Karim, A., Amis, E. J. Co-extrusion of biocompatible polymers for scaffolds with co-continuous morphology, *J. Biomed. Mater.* Res., 60, 20-29 (2002).

[26] Trifkovic, M., Hedegaard, A., Huston, K., Sheikhzadeh, M. & MacOsko, C. W. Porous films via PE/PEO cocontinuous blends. *Macromolecules* 45, 6036–6044 (2012).

[27] Pernot, H., Baumert, M., Court, F. & Leibler, L. Design and properties of co-continuous nanostructured polymers by reactive blending. *Nat. Mater.* 1, 54–8 (2002).

[28] Veenstra, H., Dam, J. Van & Boer, A. P. De. Formation and stability of co-continuous blends with a poly(ether-ester) block copolymer around its order-disorder temperature. 40, 1119–1130 (1999).

[29] Wang, J. & Mao, Q. Methodology Based on the PVT behavior of polymer for injection molding. *Adv. Polym. Technol.* 32, 474–485 (2012).

[30] Yifeng Hong and Donggang Yao, Mechanical behavior of porous polysiloxane with micropores interconnected by microchannels. *Society of Plastics Engineers* (2013).

[31] Hong, Y., Zhou, J. G. & Yao, D. Fabrication of interconnected porous elastomers by a microsphere-templating process. *Adv. Polym. Technol.* 32, 1–11 (2013).

[32] Vunjak-Novakovic, G., Maidhof, R., Marsano, A., Lee, E. J. J., *Biotechnol Progr*, 26, 565–572 (2010).

[33] Wagner, W. R., Nelson, D. M., Baraniak, P. R., Ma, Z. W., Guan, J. J., Mason, N. S., *Pharm Res-Dordr*, 28, 1282–1293 (2011).

[34] Eshelby, J. D., *Metals Trans*, 185, 806 (1949).

[35] Migneco, F., Huang, Y.C., Birla, R.K. Hollister, S.J., *Biomaterials*, 30, 6479 (2009).

[36] Jeong, C.G., Hollister, S.J., *J. Biomed. Mater*. Res. Part B, 93B, 141 (2010).

[37] Mitsak, A.G., Dunn, A.M., Hollister, S.J., J. *Mech. Behav. Biomed. Mater.*, 11, 3 (2012).

[38] D. M. Geddes, R. S. Cargill II, M. C. LaPlaca. Mechanical Stretch to Neurons Results in a Strain Rate and Magnitude-Dependent Increase in Plasma Membrane Permeability, *Journal of Neurotrauma*, Vol 20, (2013).

[39] J. A. Morehouse, D. R. Lloyd, Benny D. Freeman, Desmond F. Lawler, Kenneth M. Liechti, Eric B. Becker. Modeling the stretching of microporous membranes, *J. Membr. Sci.* 283 (2006) 430–439.

[40] J.A. Morehouse, L.S. Worrel, B. McCloskey, D.R. Lloyd, D.F. Lawler, B.D. Freeman. Impact of membrane stretching on MF performance, Presented at 15th Annual Meeting of the North American Membrane Society, Honolulu, HI, (2004).

[41] J. Morehouse. The effect of uni-axial stretching on microporous phaseseparation membrane structure and performance, Dissertation, University of Texas at Austin, (2006).

[42] J.A. Morehouse, L.S. Worrel, D.L. Taylor, D.R. Lloyd, B.D. Freeman, D.F. Lawler. The effect of uni-axial orientation on macroporous membrane structure, *J. Porous Mat.* 13 (2006) 63–75.

[43] Zhang, Bingyang. Fabrication and mechanical characterization of liquid-in-solid elastomeric soft composites. Master's Thesis, University of Illinois (2016).

[44] Dow Corning Corporation. Sylgard(R) 184 Silicone Elastomer Kit. (2015). at <http://www.dowcorning.com/DataFiles/090276fe80190b08.pdf>

[45] Owen, M. J. and Smith, P. J. Plasma treatment of polydimethylsiloxane *J. Adhes. Sci. Technol.* **8** 1063–75 (1994).

[46] Yao, M. & Fang, J. Hydrophilic PEO-PDMS for microfluidic applications. *J. Micromechanics Microengineering* **22,** 25012 (2012).

[47] Polysciences Corporation. Poly(dimethylsiloxane-b-ethylene oxide), methyl terminated. Retrieved on September 2016, at <http://www.polysciences.com/default/polydimethylsiloxane-b-ethylene-oxide-

methyl-terminated>.

[48] Contact angle. In Wikipedia. Retrieved on November 2016, at <https://en.wikipedia.org/wiki/Contact_angle>.

[49] Evans, S. D., Sharma, R., Ulman, A., Contact angle stability: reorganization of monolayer surfaces *Langmuir* **7** 156–61 (1997).

[50] Ulbrich R. R. and Bin Wadud, S. E., Determination of the linear viscoelastic region of a polymer using a strain sweep on the DMA 2980, TA Instruments Thermal Solutions (2015).

[51] Haddad, Y. M., Viscoelasticity of engineering materials, Springer, ISBN-10: 9401045550 (1995).

[52] Oliver, W. C. and Pharr, G. M. Measurement of hardness and elastic modulus by instrumented indentation: Advances in understanding and refinements to methodology. *J. Mater. Res.* **19,** 3–20 (2004).

[53] Force curve analysis, Image Metrology. Retrieved on November 2016, at <http://www.imagemet.com/WebHelp6/Default.htm#ForceCurveAnalysis/Force_Menu.htm>

[54] Bramble Berry. Production Information Sheet. (2012). at <https://www.brambleberry.com/Download.ashx?daid=2025>

[55] Ganji, F., Vasheghani-Farahani, S. & Vasheghani-Farahani, E. Theoretical Description of Hydrogel Swelling: A Review. *Iran. Polym. J.* **19,** 375–398 (2010).

[56] Ottenbrite, R. M. P., Kinam, Biomedical Applications of Hydrogels Handbook, Okano, Teruo Ed., Springer (2010).

[57] Hoffman, A. S.: Hydrogels for biomedical applications. *Adv Drug Deliver* Rev, 54, 3-12 (2002).

[58] Christensen, L. H., Breiting, V. B., Aasted, A., Jørgensen, A. & Kebuladze, I. Long-term effects of polyacrylamide hydrogel on human breast tissue. *Plastic and reconstructive surgery* **111,** 1883–1890 (2003).

[59] Sagle, A. C., Ju, H., Freeman, B. D. & Sharma, M. M. PEG-based hydrogel membrane coatings. *Polymer (Guildf).* **50,** 756–766 (2009).

[60] Nagai, K., Tanaka, S., Hirata, Y., Nakagawa, T., Arnold, M. E., Freeman, B. D., et al. *Polymer*;42:9941–8 (2001).

[61] Bird, R.B., Stewart, W.E., Lightfoot, E.N. *Transport phenomena*. 2nd ed. New York: John Wiley & Sons, Inc. (2002).